Università degli Studi di Palermo

AREA QUALITÀ, PROGRAMMAZIONE E SUPPORTO STRATEGICO
SETTORE STRATEGIA PER LA RICERCA
U. O. DOTTORATI

PhD in Biomedicine, Neuroscienc and Advanced Diagnostics
Department Biomedicine, Neurosciences and Advanced Diagnostics (Bi.N.D.)
SSD BIO/13 – Biologia Applicata

Colorectal cancer-derived small extracellular vesicles induce TGFβ1-mediated epithelial to mesenchymal transition of normal hepatocytes: new insights on pre-metastatic niche formation in the liver

Doctoral dissertation of:
Ornella Urzì

PhD Coordinator:
Prof. Fabio Bucchieri

Supervisor:
Prof. Simona Fontana

XXXV CICLO
2023

Dedicated to

My grandmother

Who

Ignited in me the passion for cancer research

Index

Abstract

More than 50% of patients affected by colorectal cancer (CRC) present liver metastasis, which is the most frequent cause of CRC-associated death. Numerous studies have shown that metastatic cascade is the result of complex mechanisms based on two-way interactions between invasive CRC cells and liver resident cells. In recent years, several findings have demonstrated that small extracellular vesicles (SEVs) released by cancer cells play a crucial role in the formation of pre-metastatic niche in the liver, specifically affecting the activities of non-parenchymal cells as Kupffer cells and hepatic stellate cells. However, although hepatocytes (heps) are the most conspicuous in the liver, their involvement in pre-metastatic niche formation remains still unknown. This study shows for the first time that SEVs derived from CRC cells (CRC_SEVs) carrying TGFβ1 impair the morphological and functional properties of human normal heps and trigger their TGFβ1-dependent epithelial to mesenchymal transition (EMT). Moreover, SEVs were also isolated from the plasma and biopsies of CRC patients. Heps treated with patients-derived SEVs underwent an EMT, thus confirming previous results. Since it is known that the EMT of heps led to the formation of a fibrotic environment, which can promote metastasis, the obtained results indicate for the first time that heps can have an active role in regulating the pre-metastatic niche formation.

Uveal melanoma (UM) is rare cancer originating from the uveal tract within the eye. Fifty percent of UM patients will develop metastatic disease, mainly in the liver; however, the reasons why the metastatic site is almost exclusively the liver are still unknown. Moreover, the role of UM-derived SEVs in initiating liver metastasis is still unknown. Similarly, to CRC-SEVs, it was found that UM-SEVs induce EMT in human normal heps.

Finally, to investigate the establishment of a fibrotic environment in CRC-SEVs-conditioned liver, a three-dimensional (3D) model, represented by liver spheroids was developed. Once characterized, liver spheroids were treated with CRC-SEVs, which decreased functional and structural markers expression, thus confirming the data obtained in 2D. Moreover, CRC-SEVs treatment increased the production of fibronectin, a known marker of fibrosis, in liver spheroids. By co-culturing metastatic CRC cells with liver spheroids, it was demonstrated that the pre-conditioning with SEVs derived by CRC cells isolated from the primary tumor strongly increased the ability of metastatic cells to invade liver spheroids. Collectively these data shed the light on mechanisms involved in the formation of the pre-metastatic niche in the liver, demonstrating that heps actively participate in this process. This evidence may help to find new therapeutic opportunities to counteract liver metastasis of CRC.

1. Introduction

When in 1996 Raposo et al. discovered that extracellular vesicles (EVs) from immune cells are capable of presenting antigens [1], thus giving the first evidence that EVs have a role in cell-cell communication, the interest of the scientific community increased exponentially. In the past two decades, several studies demonstrated how EVs take part both in physiological and pathological processes, playing a key role in many diseases, including cancer. Nowadays, it is well established that EVs are involved in each step of cancer progression, from tumor growth to metastatic spreading. In particular, EVs are involved in the formation of the so-called "pre-metastatic niche", a microenvironment favourable to the establishment and growth of metastases. Some studies highlighted that EVs released by colorectal cancer cells can favour liver metastasis affecting the functions of liver non-parenchyma cells. However, in this process, the role of hepatocytes, which represent the most represented cells in the liver parenchyma, is still unknown.

1.1 Cancer and metastasis

Cancer is a pathological condition characterized by the uncontrolled proliferation of cells that can infiltrate normal organs and tissues of the body and alter their structure and function [2]. As mentioned by Francis Peyton Rous, a tumor virologist, Nobel lecture, in 1966:

"*Tumors destroy man in a unique and appalling way, as flesh of his own flesh which has somehow been rendered proliferative, rampant, predatory and ungovernable. They are the most concrete and formidable of human maladies, yet despite more than 70 years of experimental study they remain the least understood.*"

Although several factors, including genetics, epigenetics, environment, nutrition, and physical activity, can affect the onset of cancer [3], the majority of cancers (about 90-95 %) are due to genetic mutations from environmental and lifestyle factors [4].

Despite more than 100 types of cancer can affect humans, all tumor cells possess the six hallmarks of cancer, described by Douglas Hanahan and Robert Weinberg in 2000 [5]:

1. Sustaining proliferative signaling
2. Evading growth suppressors
3. Resisting cell death
4. Enabling replicative immortality
5. Inducing/accessing vasculature
6. Activating invasion and metastasis

Some years later, tow new hallmarks were included: deregulating cellular metabolism and avoiding immune destruction [5].

However, since these hallmark traits, on their own, fail to address the complexities of cancer pathogenesis last year they introduced a new concept: the "enabling characteristics". Douglas Hanahan and Robert Weinberg defined enabling characteristics as consequences of the aberrant condition of neoplasia that provide the means by which cancer cells and tumors can adopt these functional traits. The two enabling processes were genome instability and tumor-promoting inflammation (Fig. 1) [6].

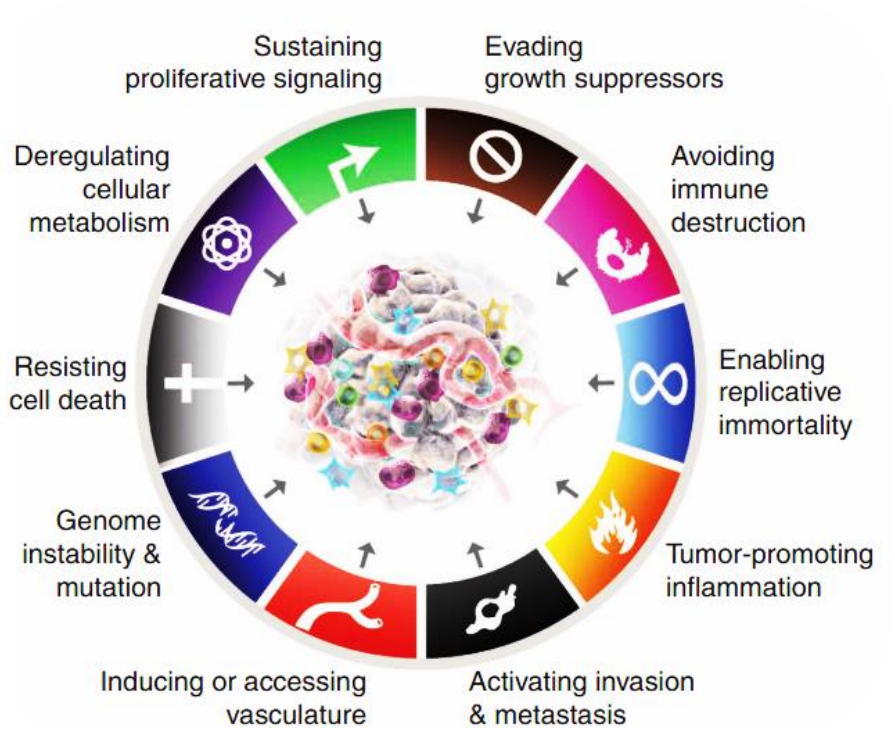

FIGURE 1 The 8 hallmarks of cancer and the 2 enabling characteristics [6]

One of the most well-known properties of cancer cells is their ability to invade neighboring tissues; invasive capability is the property that enables the dissemination of tumor cells around the body. Many types of tumors eventually release cancer cells that migrate to distant sites in the body, through the blood or lymph system, where they form the secondary tumors known as metastases [7]. Despite the development of technologies and therapeutic strategies, metastasis is still the major cause of cancer-related death today [8].

To acquire the ability to metastasize cancer cells have to undergo a multitude of phenotypic changes, in a multistep process that starts with local invasion of the cells into the surrounding tissues. They then have to invade blood vessels, survive in the harsh environment of the circulatory system, exit this system and then start dividing in the new tissue (Fig. 2) [5, 9].

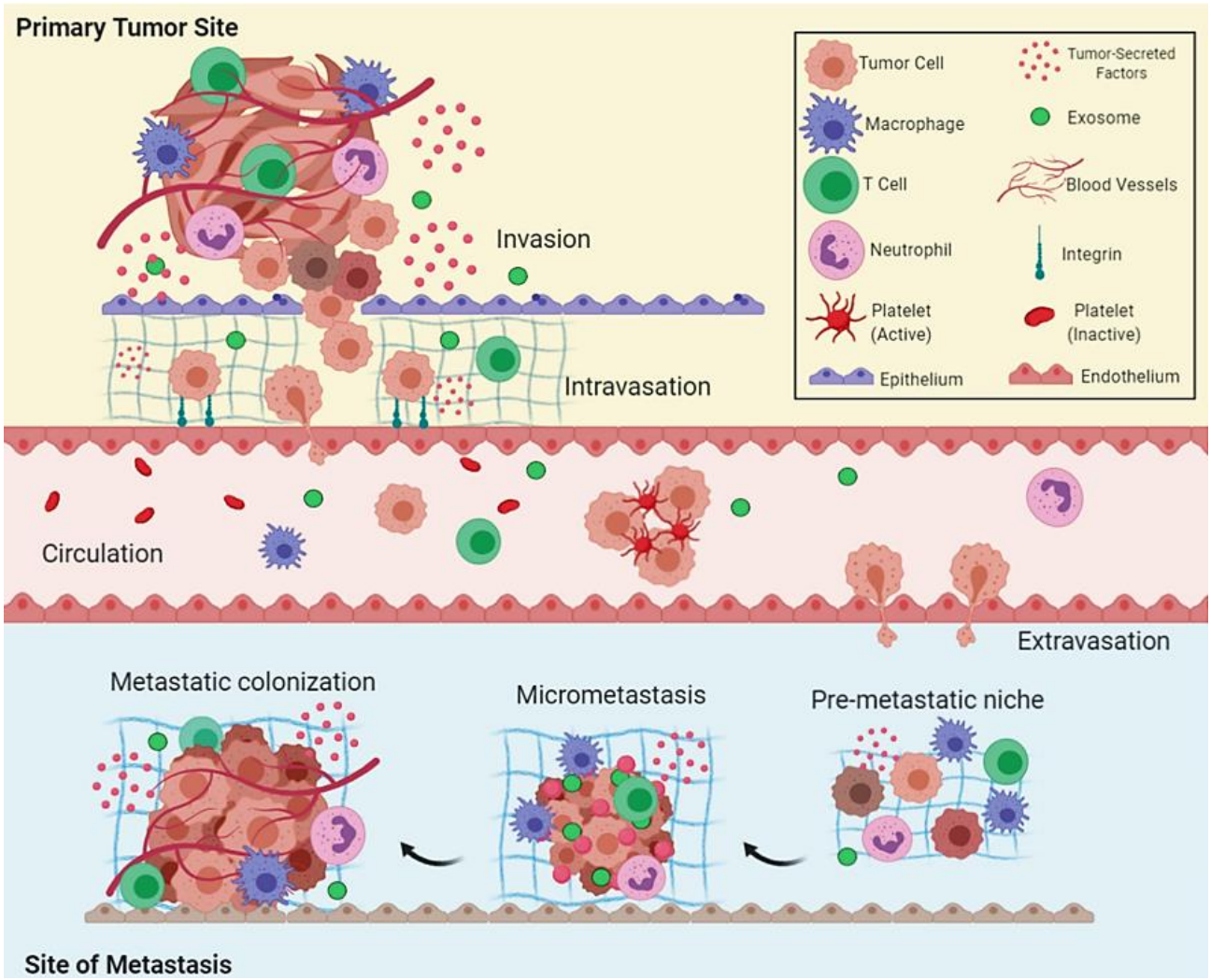

FIGURE 2 Overview of the metastatic cascade: The five key steps of metastasis include invasion, intravasation, circulation, extravasation, and colonization [10]

In 1889, Stephen Paget formulated the hypothesis of "seed and soil", in which cancer cells represent the "seeds" that can go in all directions but will only take root in congenial "soil" [11]. Several clinical observations supported this hypothesis, highlighting that most cancers metastasize to specific organs, following a process known as "organotropism" (Fig. 3). While prostate cancer preferably metastasizes in bone [12], uveal melanoma typically colonizes the liver [13]. Breast cancer, instead, can relapse in different organs, such as bone, lung, liver, and brain [14].

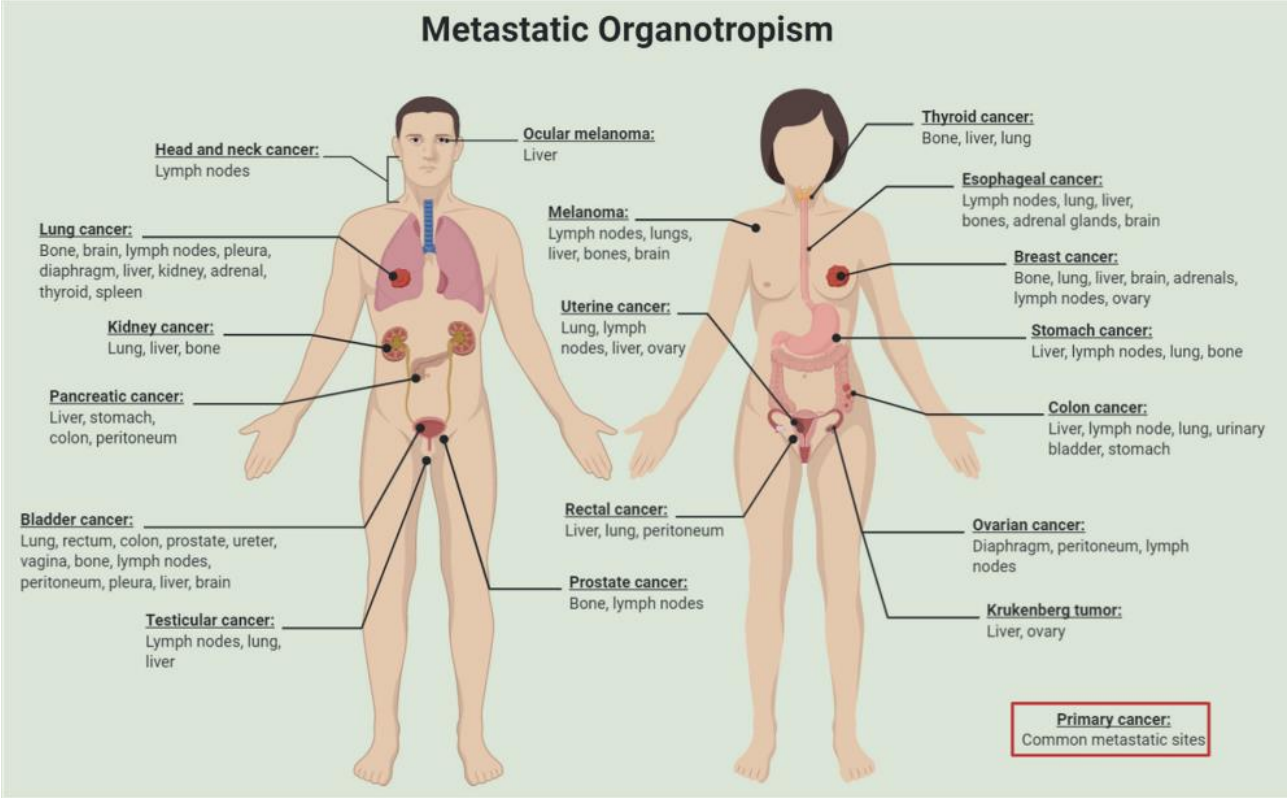

FIGURE 3 Metastatic Organotropism: clinical observations suggest that most cancers metastasize to specific target organs, a process known as "metastatic organotropism" [10]

Metastatic organotropism can be regulated by multiple factors, including the circulation pattern, tumor-intrinsic factors, organ-specific niches, and the interaction between tumor cells and the host microenvironment [15]. In this context, the concept of "pre-metastatic niche" was conceptualized, as a fertile "soil" conducive to the survival and outgrowth of metastatic "seed" [16]. The formation of the pre-metastatic niche is the very first step of metastatic spreading and precedes the arrival of metastatic cancer cells. Cells from the primary tumor release soluble factors and extracellular vesicles that trigger crucial steps of pre-metastatic establishments, such as the alteration of local resident cells, the recruitment of non-resident cells, and the recruitment of circulating cancer cells [17-19]. The main features of the pre-metastatic niche are increased vascular permeability, ECM remodeling, angiogenesis, and immunosuppression [20].

1.2 Colorectal cancer

Colorectal cancer (CRC) is the development of cancer in the colon or rectum, and it's characterized by different symptoms, including blood in the stool, weight loss, and fatigue [21]. CRC is the third leading cause of cancer-related deaths in both genders worldwide [22], and it's correlated with old age, obesity, smoking, and lack of physical activity [23].

It has been found that some dietary factors, such as red meat, processed meat, and alcohol, can increase the risk of CRC [24]. Another risk factor is represented by inflammatory bowel disease, including Crohn's disease and ulcerative colitis [25].

CRC develops following a predictable progression of histological and concurrent epigenetic and genetic changes which originate in the epithelial cells of the colon, that frequently increase the Wnt signaling pathway activity [26]. In the 'classic' CRC formation model, cancer arises from a polyp beginning with an aberrant crypt, which then evolves into an early adenoma. Then, the adenoma progresses to an advanced adenoma before finally transforming into a tumor. This process is driven by an accumulation of mutations and epigenetic alterations and can take 10–15 years to occur (Fig. 4) [27]. Currently, two sequences describing progression from normal colon to CRC have been identified depending on the first mutation which occurs most frequently in adenomatous polyposis of colon (APC) gene and β-catenin (CTNNB1) gene and leads to hyperplasia [28]. Next, the occurrence of mutations in NRAS, KRAS, and BRAF genes induces the transition by early to advanced polyps. Subsequent alterations in SMAD4 and PI3KCA induce the formation of early cancer which progresses to advanced cancer with other mutations in TP53 and TGFBR2 genes [26].

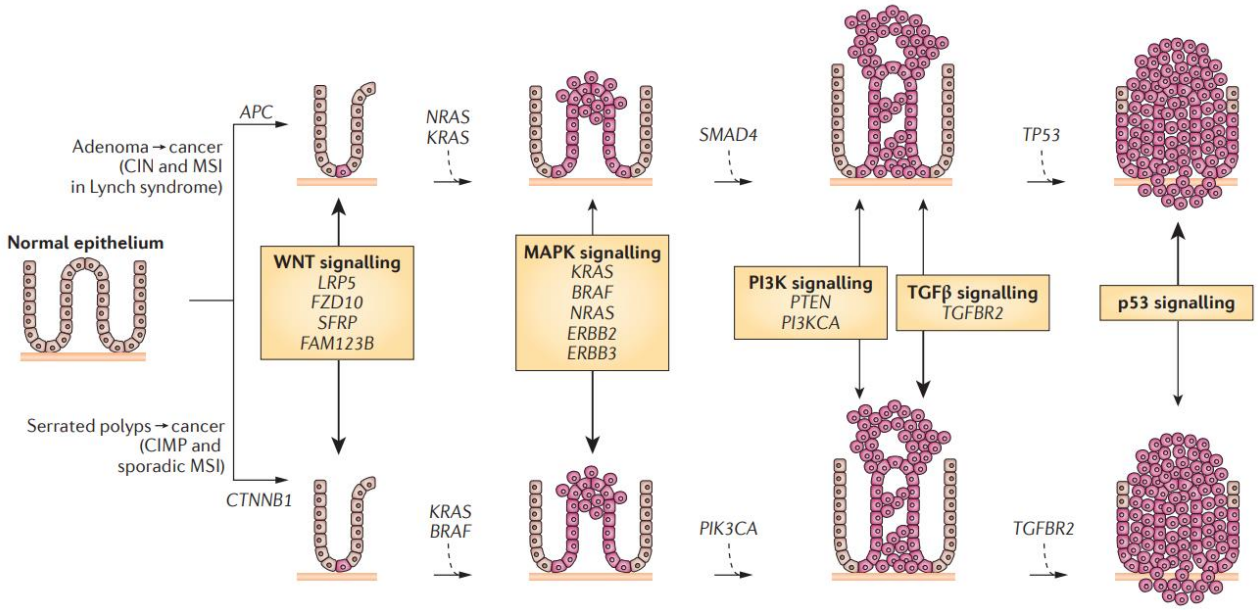

FIGURE 4 The polyp to colorectal cancer sequences [26]

The prevalence of CRC has been dramatically growing at an alarming rate globally in recent years. CRC incidences vary by country, the highest number of CRC new cases was estimated in China and the USA in 2020, and this number is expected to grow continuously over the next 20 years [22]. Together with the USA and China, the top 10 countries are Brazil, France, UK, Italy, Germany, India, Russia, and Japan (Fig. 5).

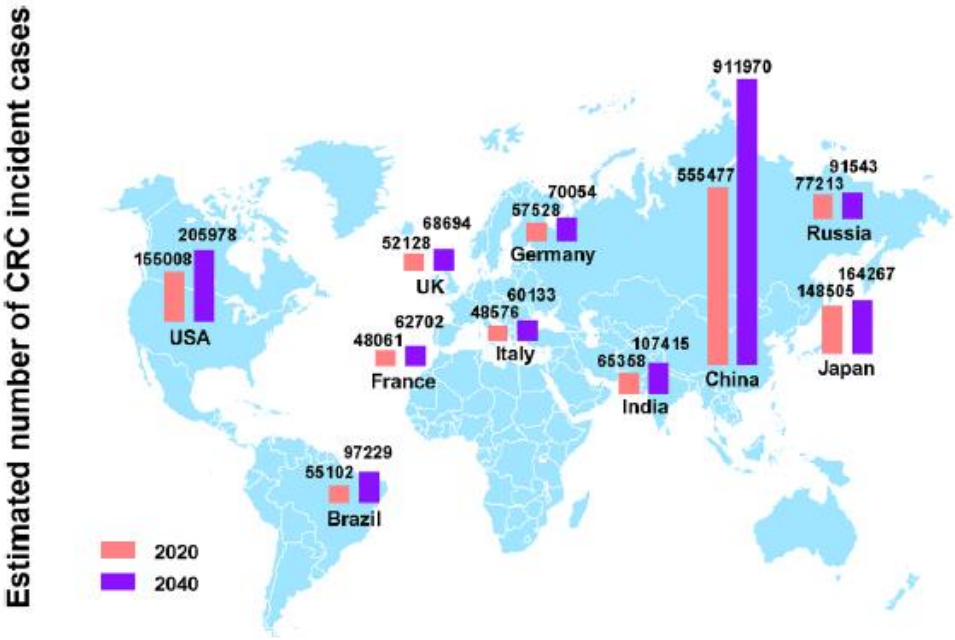

FIGURE 5 The number of new CRC cases in the top 10 countries with the highest incident cases in 2020 and projections for 2040 [22]

To date, treatments for primary and metastatic colorectal cancer include chemotherapy, targeted therapy, immunotherapy, surgery, and radiation therapy [29]. The 5-year survival of CRC patients is 65% if the tumor is localized or regional; however, if cancer has spread to distant parts of the body the survival of CRC patients can be dramatically reduced, reaching 15%, thus making metastasis the main complication of CRC [30].

1.3 CRC Metastasis to the Liver

As discussed above, the choice of metastatic site formation is not random; in the case of colon cancer, the liver represents the most common site of metastases [30]. Approximately 50% of patients with CRC will develop liver metastasis during their life [31]. Metastasis of CRC in the liver has been explained in past years due to the portal vein system, which directly connects the colorectal and liver.

The metastatic dissemination of CRC cells in the liver is a complex and multi-step process (Fig. 6):

1. morphological changes such as EMT confer to a small number of CRC cells the capacity to evade the primary tumor;
2. CRC cells migrate through the ECM and invade the neighboring tissues;
3. intravasation of CRC cells and survival in the circulation;
4. extravasation of CRC cells;
5. colonization to liver forming CRC metastasis

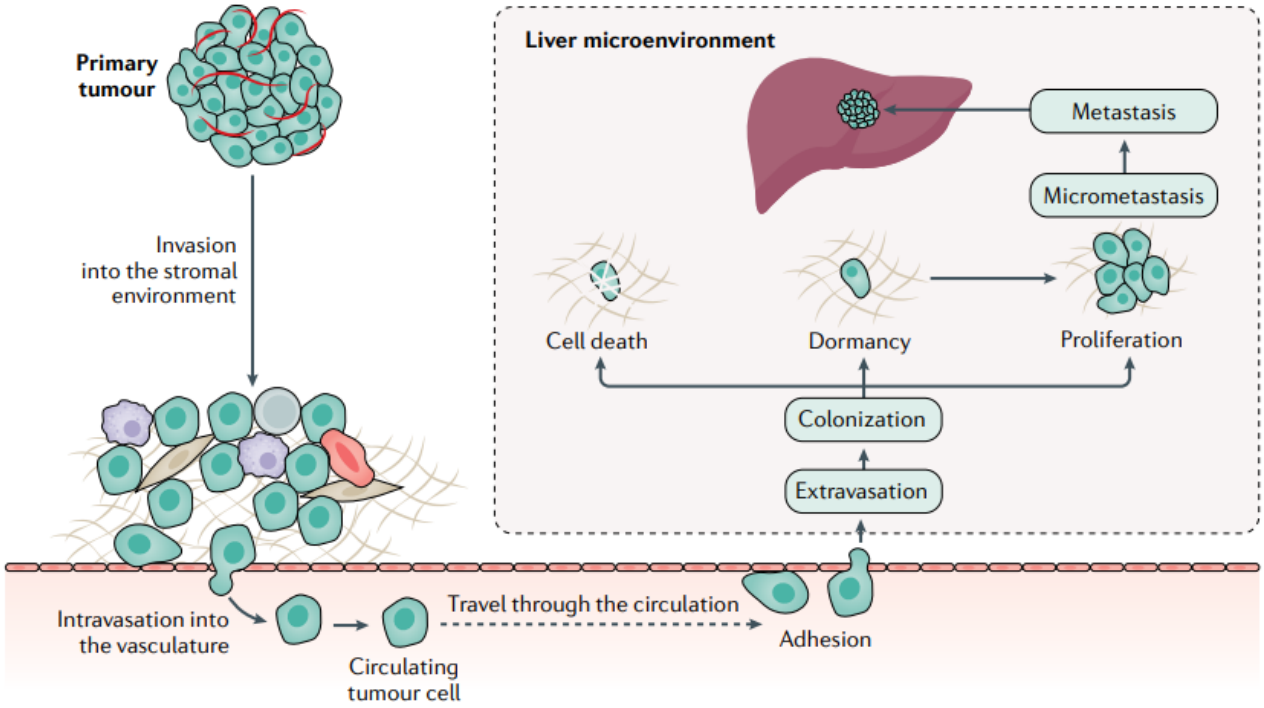

FIGURE 6 Metastatic invasion of tumour cells into the liver [32]

The formation of CRC liver metastasis involves the activation of several biomolecules, including non-coding RNAs (ncRNAs), Notch pathway, TGFβ signaling, Tyrosine kinase c-MET signaling, phosphatase of regenerating liver (PRL3), tumor-associated calcium signal transducer 2 (Trop-2) and so on [33]. Moreover, CRC cells, even before their arrival in the metastatic site, produce and release many soluble factors, such as cytokines, chemokines, and extracellular vesicles, which modify the liver microenvironment making it supportive for metastasis [34, 35].

Once metastatic CRC cells reach the liver, they encounter a unique subset of highly specialized resident cells, including hepatocytes, Kupffer cells, hepatic stellate cells, dendritic cells, and resident natural killer cells [36].

The complex network of interactions established between CRC cancer cells and liver resident cells can deeply modify the phenotype of hepatic cells. For instance, although in the early phase of the metastatic invasion, Kupffer cells are predominantly tumoricidal [37], they can promote metastasis after extravasation by releasing growth factors (HGF and VEGF) which enhance cancer cell proliferation and angiogenesis [38].

Even though to date CRC patients can benefit from a multidisciplinary team to determine an optimal personalized therapeutic approach, liver metastasis remains the main cause of death in these patients [32]. For this reason, revealing the molecular mechanisms involved in the early step of CRC liver metastasis formation is crucial to allow early detection and the development of effective therapies.

1.4 TGF-β signaling

Transforming Growth Factor-β (TGF-β) family includes TGF-β1, TGF-β2, and TGF-β3, which regulate many processes such as cellular proliferation, survival, migration, and differentiation [39]. TGF-β signaling can occurs through canonical small mothers against decapentaplegic homolog (SMAD) signaling and through crosstalk non-canonical signaling pathways. The canonical TGF-β signaling pathway is activated upon TGF-β binding to two serine/threonine kinase receptors TGF-β type II receptors (TβRII), leading to the recruitment and formation of a heteromeric complex with 2 TGF-β type I receptors (TβRI). TβRII kinase phosphorylates TβRI, which in turn phosphorylates the SMAD proteins SMAD2 and SMAD3. This induces the assembly into heterodimeric and trimeric complexes with SMAD4, which translocate to the nucleus to regulate expression of TGF-β target genes. SMAD signaling induces a negative feedback loop through SMAD7, which mediates TβRI degradation.

Besides canonical signaling, TGF-β can induce various non-canonical signaling pathways resulting in changes in transcription, the cytoskeleton, tight junctions, and translation. Non-canonical pathways include, for example, Rho/Rho-associated coiled-coil kinase (ROCK) signaling, phosphoinositide 3-kinase/AKT signaling, or the activation of multiple mitogen-activated protein kinases (MAPK), including extracellular signal-regulated kinases (ERK), through Ras activation, and c-Jun N-terminal kinases (JNK) and p38 (Fig. 7).

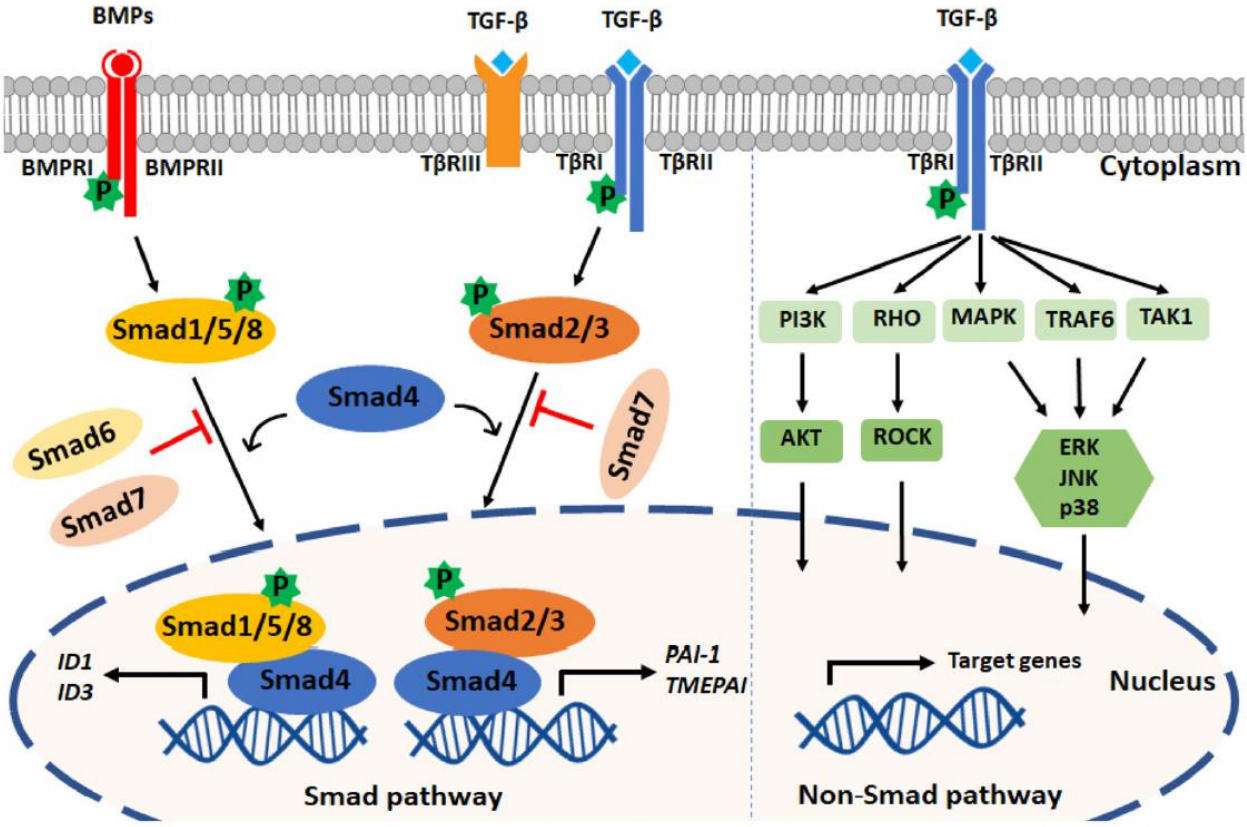

FIGURE 7 TGF-β signaling pathways. (left panel) Canonical signaling pathway. Upon ligand engagement, the type II kinases phosphorylate the type I receptors, which are then activated. TGF-β induces the phosphorylation of Smad2/3. By forming complexes with Smad4, phosphorylated Smad2/3 translocate into the nucleus to regulate target gene expression. PAI1 and TMEPAI are typical target genes induced downstream of Smad3 phosphorylation. Inhibitory Smads (i.e. Smad7) can antagonize the action of signal-transducing Smad4. (right panel) Non-canonical signaling pathways. TGF-β family members can also activate PI3K, RHO, MAPK, TRAF6, and TAK1 [40].

In the liver, TGF-β1 is mainly expressed by Kupffer cells and stellate cells, while is not expressed by hepatocytes. However, TGF-β is a key inducer of fibrosis, activating hepatic stellate cells and transdifferentiating hepatocytes toward myofibroblasts through an epithelial to mesenchymal-like process [41]. The activation of TGF-β signaling pathway causes an increase of matrix deposition through connective tissue growth factor (CTGF), receptor for activated c kinase 1 (RACK1) and NADPH oxidase 4 (Nox4), and collagen-1 secretion. The establishment of a fibrotic environment promotes the appearance of liver metastases and predicts the occurrence and relapse of metastatic disease [42-44]. In colorectal cancers, metastases are characterized by high stroma and TGF-β signaling, resulting in poor prognosis [45]. Many studies demonstrated that TGF-β play an important role in creating the fibrotic niche; besides TGF-β supports immune escape, angiogenesis, and tumor outgrowth in different phases of liver colonization [46-48].

TGF-β is definitely the master regulator of epithelial to mesenchymal transition, which is a part of the dynamic plasticity of cancer cells [49].

1.5 Epithelial to mesenchymal transition

Epithelial to mesenchymal transition (EMT) is characterized by the loss of epithelial cell character, cell polarity, and cell-cell junctions, and the gain of mesenchymal features, resulting in more invasive potential [46]. Multiple factors and signals accurately regulate EMT at different levels. The most well-known mediators of EMT are cytokines, such as TGF-β, fibroblast growth factor (FGF) family, epidermal growth factor (EGF), and hepatocyte growth factor (HGF) [50, 51].

As shown in Fig. 8, epithelial cells display apical-basal polarity, are held together by tight junctions, adherens junctions, and desmosomes, and are anchored to the basement membrane by hemidesmosomes. Epithelial cells express molecules associated with the epithelial state, which help to maintain cell polarity. The induction of EMT is triggered by specific transcription factors, including ZEB, SNAIL, and TWIST, which repress the expression of epithelial state genes and increase the expression of genes associated with the mesenchymal state. These changes in gene expression result in the breakdown of cell-cell junctions and the loss of apical–basal cell polarity.

At the same time, cells acquire mesenchymal-like features, such as front-to-back polarity and invasive capacities. EMT is a reversible process, and mesenchymal cells can revert to the epithelial state by undergoing mesenchymal to epithelial transition (MET). EMT and MET occur during normal development and during cancer progression.

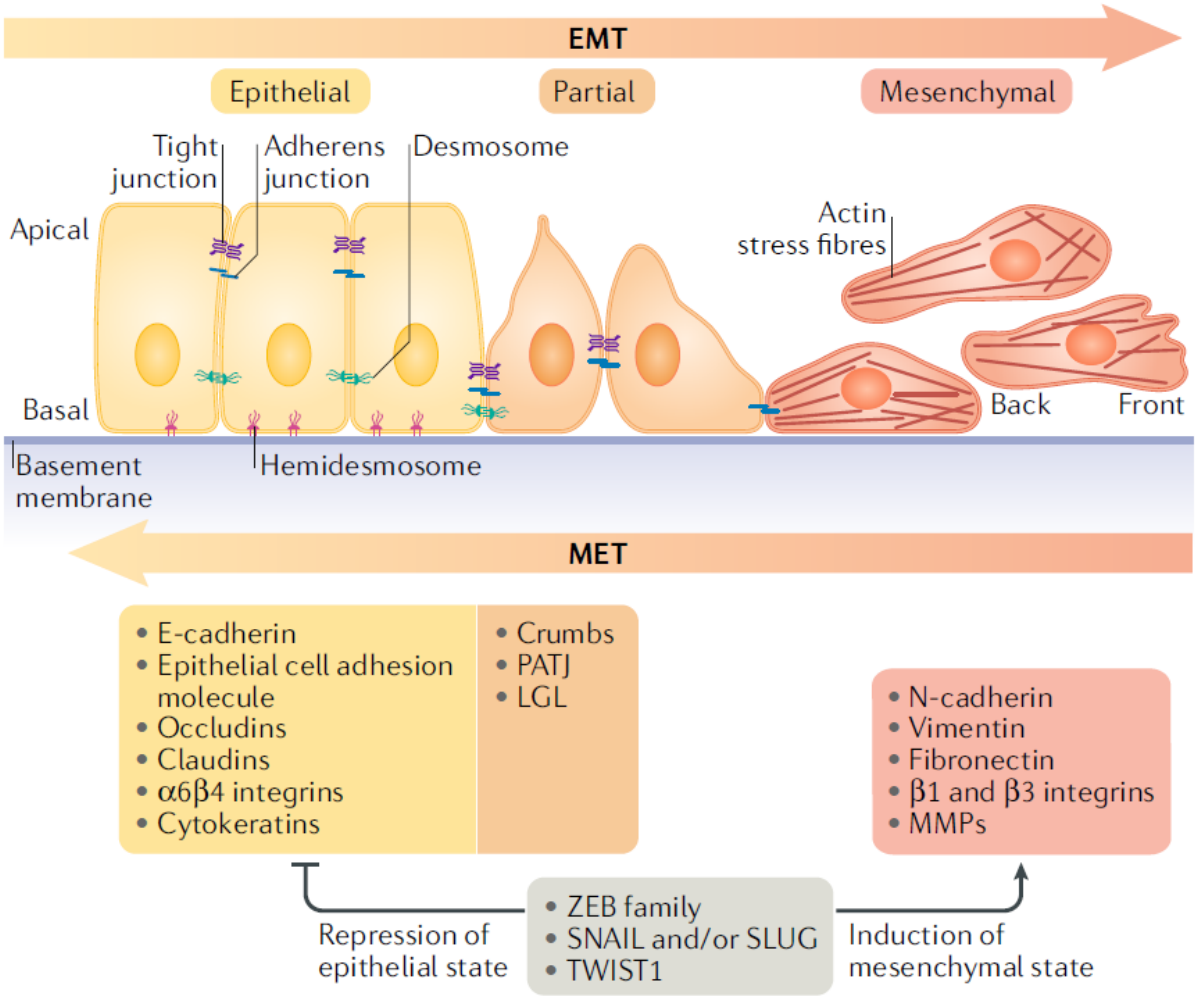

FIGURE 8 Outline of a typical epithelial to the mesenchymal transition program. Epithelial cells express molecules associated with the epithelial state, which help to maintain cell polarity (listed in the yellow and light orange boxes). EMT is activated by transcriptional factors (listed in the grey box) that repress the expression of epithelial molecules and concomitantly activate the expression of genes associated to a mesenchymal state (listed in red box) [52]

In the liver, EMT has been extensively studied and it is believed that it could be strongly involved in liver fibrosis thus representing a possible therapeutic target for limiting the fibrotic process [53]. Since as mentioned above, fibrosis favors metastatic cascade, a better understanding of the correlation between EMT and fibrosis may allow the development of new therapeutic strategies.

Among the soluble factors which take part in the regulation of these processes, extracellular vesicles may play a key role [54].

1.6 Extracellular vesicles

Although considered as garbage bind when discovered [55], extracellular vesicles (EVs) are now recognized as one of the most attractive mechanisms of cell-cell communication [56]. EVs are nanosized lipid-bound particles released by almost all cell types in the extracellular space. Their complex content reflects the cell of origin and includes proteins [57], lipids [58], metabolites [59], and nucleic acids, as DNA [60], mRNA [61], microRNA [62], and lncRNA [63] (Fig. 9).

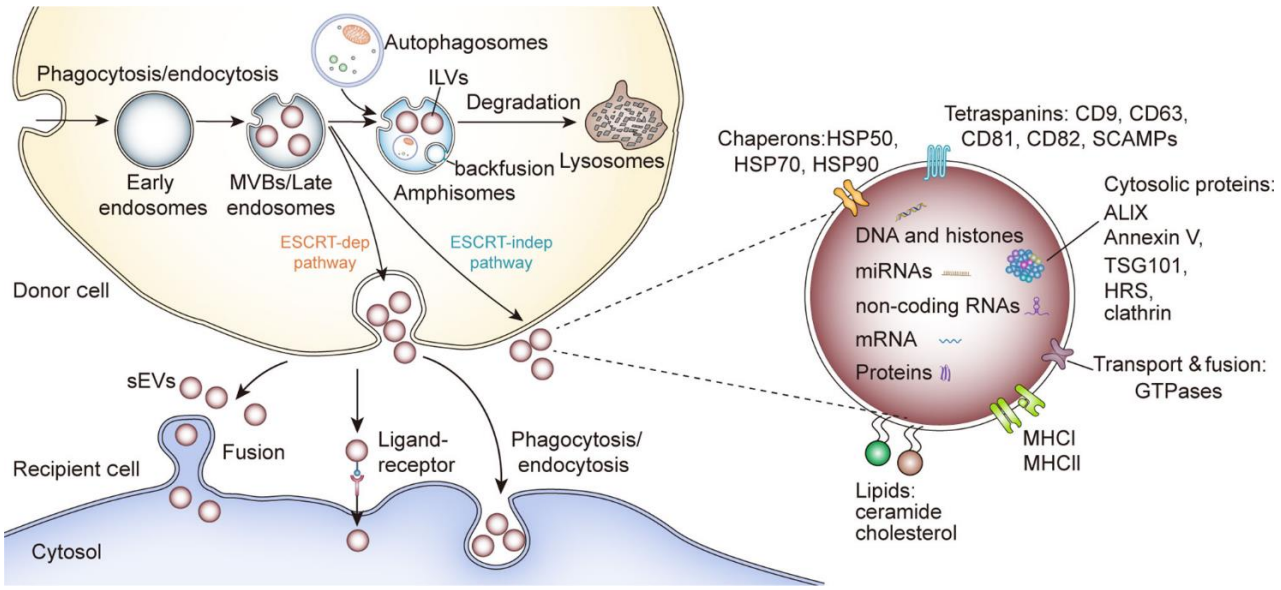

FIGURE 9 EVs biogenesis, cargo, and internalization by target cell [64]

In 2007, Valadi et al. showed for the first time that EV content can be functionally transferred to target cells thus modulating their phenotype. They demonstrated that EVs mediate genetic exchange between cells by releasing functional microRNA and mRNA into receiving cells [61]. This observation was followed by an increasing number of studies that unquestionably demonstrated the involvement of EVs in cell-cell communication taking part in both physiological and pathological processes.

Moreover, since EVs can be isolated from several bio-fluids including blood [65], saliva [66], urine [67], cerebrospinal fluid [68], seminal fluid [69], breast milk [70] and so on they have been considered as possible biomarkers [71]. Although they can be isolated using different techniques, the most used method of EV isolation is ultracentrifugation. Other techniques include density gradient centrifugation, size exclusion chromatography, and polymer-based precipitation, with each varying in yield of EVs, the depletion of contaminants, the intensity of labour, time, and the cost of the procedure. Since they attracted the attention of the scientific community, the number of studies regarding EVs is growing exponentially.

Several molecules have been identified as EV markers, such as tetraspanins (CD9, CD63, CD81), heat shock protein (Hsp70, HSP90), ALG-2-interacting protein X (Alix), tumor susceptibility gene 101 (Tsg101), and Major Histocompatibility Complex (MHC class I and II) [72].

In the past, EVs have been classified, according to their biogenesis, into exosomes, ectosomes, microvesicles, and apoptotic bodies [73]. Exosomes are the smallest EVs (~40-120 nm in diameter) and they originate from the endosomal compartment following the fusion of multivesicular bodies with the cell membrane [74]. Ectosomes, whose size range 100-500 nm [75] and microvesicles, usually from 100 nm to 1 μm in diameter, are formed directly by the outward budding of the plasma membrane [76]. Finally, apoptotic bodies are the largest EVs, ranging from ~500 nm to 5 μm, and are released as a consequence of programmed cell death [77]. However, as demonstrated in many studies [78, 79], the existing overlap among different EV subpopulations and the difficulty to clarify their biogenesis prompted the scientific community to simplify their classification into small (< 200 nm) and large (> 200 nm) EVs [80].

Nowadays, it is clear that EVs are strongly involved in the income of many diseases, such as neurological diseases [81], cardiovascular diseases [82], metabolic disorders [83], and cancer [84].

1.7 Tumor-derived extracellular vesicles

Increasing evidence has demonstrated that EVs are involved in several steps of cancer, from tumor initiation to angiogenesis, immune escape, and metastatic dissemination (Fig. 10). Many studies demonstrated that the inhibition of EV release from cancer cells was associated with reduced cancer growth and metastasis [85-87], thus highlighting that EVs play a key role in cancer development. Moreover, highly aggressive cancer cells produce more EVs than less aggressive cancer cells or normal cells [88]. Since it is known that EV content reflects the cell of origin, tumor-derived EVs (TD-EVs) carry several biomolecules that can be transferred into recipient cells, thereby altering their phenotype. For instance, glioma- and breast cancer-derived EVs altered the phenotype of non-transformed cells, leading them to acquire some phenotypic features of a transformed cell, such as increased growth and survival [89]. Besides, Schillaci et al. demonstrated that metastatic CRC cells can transfer their amoeboid phenotype to isogenic primary cancer cells through EVs [90].

In the context of an expanding tumor, cancer cells have to remain viable despite being exposed to a stressful environment with limiting amounts of nutrients and oxygen. The release and transfer of EVs between cancer cells may serve as a survival mechanism because cancer cells can consistently promote the survival of other cancer cells through EVs [91].

Moreover, EVs are involved in chemoresistance as demonstrated by Kreger et al., who found that breast cancer cells treated with paclitaxel (PTX), a known anti-tumor drug [92], produced an high number of EVs containing survivin (protein involved in cell survival) [91].

EVs have been demonstrated to also promote tumor angiogenesis. For example, it was shown that cancer-derived EVs carried EGF-receptor and increased the production of VEGF in human umbilical vein endothelial cells, thus stimulating blood vessel formation [93].

Cancer cells mediated immunosuppression typically through the increased expression of programmed death-ligand 1 (PD-L1) on the surfaces of cancer cells, thus leading to the generation of several inhibitors [94]. The development of immunotherapeutic drugs, based on immune checkpoint inhibitors, revolutionized cancer therapies and increased the survival of cancer patients. However, as for chemotherapeutic drugs, also immunotherapies could lead to chemoresistance. Interestingly, it has been demonstrated that EVs are involved in this mechanism since they can carry PD-L1 on their surface [95], thus limiting the effects of anti-PD-L1 therapies [96].

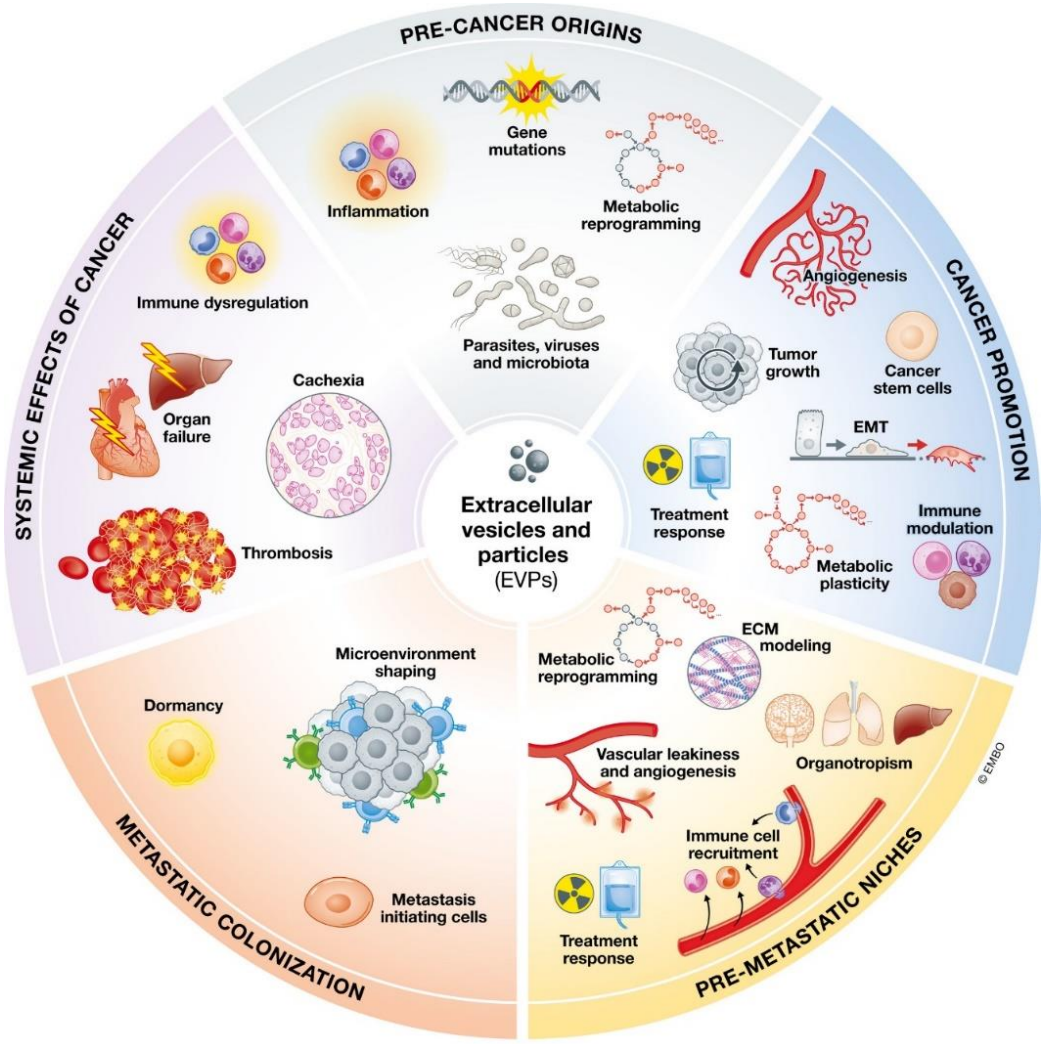

FIGURE 10 Diagram depicting the contribution of EVs to different aspects of cancer initiation and progression [97]

1.8 TD-EVs as regulators of metastatic cascade

Even before their arrival, tumor cells can induce pre-metastatic niche formation in distant organs by releasing soluble factors that encourage their survival, attachment, invasion, immune evasion, and outgrowth [16]. Many studies highlighted that TD-EVs carry proteins and microRNAs that reprogramme or educate target cells towards a pro-metastatic and proinflammatory phenotype [16, 87, 98]. Interestingly EVs can dictate metastatic organotropism (Fig. 11) [99]. Breast and pancreatic cancer cell-secreted EVs express integrins on their surface, which promotes their homing to specific organs thereby preparing the pre-metastatic niche [100]. In particular, the presence of $\alpha_6\beta_4$ heterodimer on the EV surface favoured the homing to the lungs, while $\alpha_v\beta_5$ to the liver [100]. EVs released by melanoma cells re-educate bone marrow-derived cells, thus contributing to the formation of the pre-metastatic niche in the lungs [87]. Pancreatic cancer cells produce EVs containing MIF, which promote TFGβ expression in Kupffer cells, stimulating hepatic stellate cells to secrete fibronectin thus promoting the establishment of liver pre-metastatic niche [98].

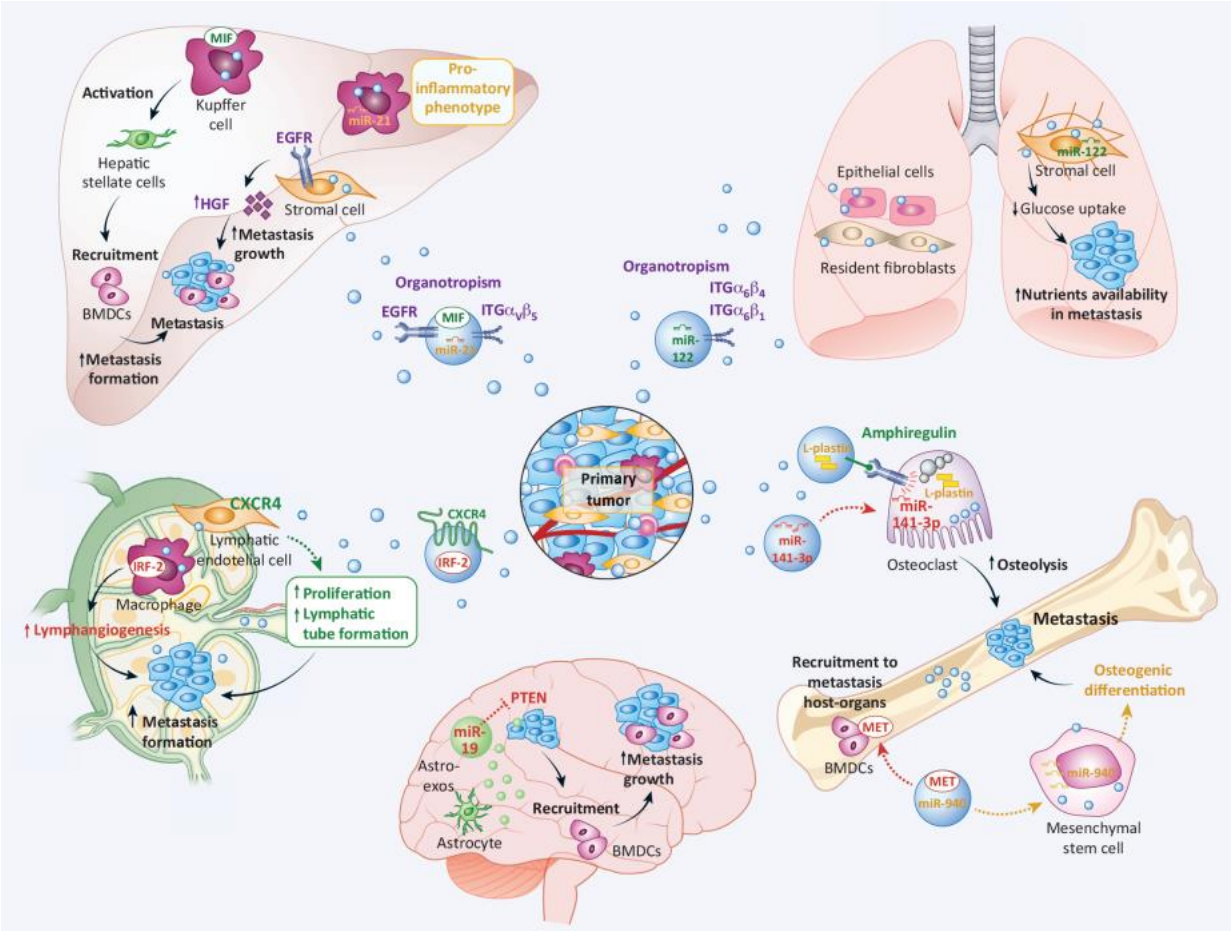

FIGURE 11 EVs can dictate metastatic organotropism [99]

Recent evidence shed the light on the role played by CRC-derived EVs in the pre-metastatic niche formation in the liver. Tian et al. demonstrated that CRC EVs carry miR-121 and miR-122 that suppressed Serine Peptidase Inhibitor, Kunitz Type 1 (SPINT1) and promoted hepatocyte growth factor (HGF) expression in liver stromal cells which contributes to the pathogenesis of liver metastasis [101]. Another group demonstrated that CRC-EVs are enriched in miR-21-5p, which promoted a liver proinflammatory phenotype. CRC-sEVs carrying miR-21-5p polarized liver macrophages by increasing the expression of pro-inflammatory cytokines, such as TNF-α and IL-6, both *in vitro* and *in vivo* [102]. Shang et al. highlighted that CRC-EVs, carrying miR-183-5p, downregulated FOXO1 expression and enhanced proliferation, invasion, and tube formation abilities of endothelial cells; their findings were also confirmed in vivo suggesting that CRC-derived EVs promote angiogenesis [103]. CRC-EVs may target also cancer associated fibroblasts and alter their lipid metabolism promoting liver metastasis [104]. Other studies demonstrated that CRC-EVs can promote M2 polarization [105, 106].

Overall, this evidence suggests that CRC-EVs participate in the pre-metastatic niche formation by affecting the phenotype of liver non parenchyma cells; however, no studies in literature focused on the effect of CRC-EVs on the main cell type in the liver: hepatocytes.

2. Aim of the study

In the last years, many studies highlighted the role of CRC-derived EVs in the formation of the pre-metastatic niche in the liver at the level of non-parenchyma cells, such as macrophages and hepatic stellate cells. However, although hepatocytes represent the most prominent part of the liver they have been described to be involved only in the late steps of the metastatic cascade. To date, the role of hepatocytes in the early steps of metastasis, in particular during the pre-metastatic niche formation, is still unknown.

The aim of this work was to study the effects induced by CRC-derived small EVs on structural features and functional activities of hepatocytes, and then how CRC-SEVs can be involved in the regulation of liver metastasis progression, specifically evaluating their involvement in pre-metastatic niche formation (Fig. 12).

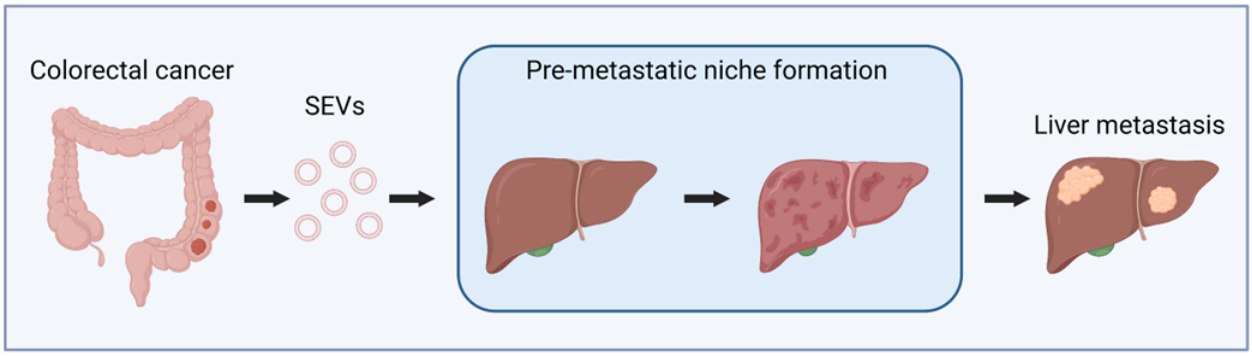

FIGURE 12 Schematic illustration of the aim of this study. Colorectal cancer cells release small extracellular vesicles (SEVs) that may participate in the formation of pre-metastatic niche in the liver, thus favoring liver metastasis. SEVs: small extracellular vesicles.

3. Materials and Methods

3.1 Cell cultures

3.1.1 THLE-2 cells

SV40 large T antigen-immortalized normal human liver epithelial cell line, THLE-2 (ATCC, Manassas, VA), was cultured in Airway Epithelial Cell Basal Medium (ATCC, Manassas, VA) with the Bronchial Epithelial Cell Growth Kit (ATCC, Manassas, VA), supplemented with 70 ng/ml phosphoethanolamine, 5 ng/ml epidermal growth factor (EGF), 10% heat-inactivated fetal bovine serum (FBS), 100 U/mL penicillin, and 100 µg/ml streptomycin (Euroclone, UK) at 37 °C with 5% CO2. Cells were maintained in pre-coated flasks with a collagen coating made with a mixture of 0.01 mg/ml fibronectin (Sigma-Aldrich, St Louis, MO, USA), 0.03 mg/ml bovine collagen type I (Advanced Biomatrix, San Diego region, California, USA), and 0.01 mg/ml bovine serum albumin (Sigma-Aldrich, St Louis, MO, USA).

To obtain liver spheroids, THLE-2 cells were cultured in LHC8 medium (Gibco) supplemented with 70 ng/ml phosphoethanolamine, 5 ng/ml epidermal growth factor (EGF), 10% heat-inactivated FBS, 100 U/mL penicillin, and 100 µg/ml streptomycin (Euroclone, UK) at 37 °C with 5% CO2. Cells were maintained in pre-coated flasks with a collagen coating made with a mixture of 0.03 mg/ml bovine collagen type I (Advanced Biomatrix, San Diego region, California, USA), and 0.01 mg/ml bovine serum albumin (Sigma-Aldrich, St Louis, MO, USA). We found that these culturing conditions allow the maintenance of healthy hepatocytes in a low differentiated state, which is useful in the starting steps of spheroids formation. THLE-2 cells were seeded into ultra-low attachment 96 well plates (1.500 cells per well) in 100 µl of LHC8 complete media. After 3 days, 100 µl of Airway Epithelial Cell Basal Medium (ATCC, Manassas, VA) supplemented with 2X Bronchial Epithelial Cell Growth Kit (ATCC, Manassas, VA) 70 ng/ml phosphoethanolamine, 5 ng/ml epidermal growth factor (EGF), 100 U/mL penicillin, and 100 µg/ml streptomycin (Euroclone, UK) without FBS were added to each well. On day 4 and day 5, a half change of media was performed, by discarding 100 µl of media from each well and adding 100 µl of fresh Airway Epithelial Cell Basal Medium (ATCC, Manassas, VA) supplemented with Bronchial Epithelial Cell Growth Kit (ATCC, Manassas, VA) 70 ng/ml phosphoethanolamine, 5 ng/ml epidermal growth factor (EGF), 100 U/mL penicillin, and 100 µg/ml streptomycin (Euroclone, UK) without FBS. On day 7 the spheroids were collected for further analyses.

3.1.2 SW480 and SW620 cells

The colorectal cancer cell lines SW480 (ATCC CCL-228) and SW620 (ATCC CCL-227) are isogenic cell lines derived respectively from the primary tumor and from lymph nodes.

They were maintained in RPMI 1640 medium (Euroclone, UK) supplemented with 10% heat-inactivated FBS (Euroclone UK), 2mM L-glutamine (Euroclone, UK), 100 U/ml penicillin, and 100 µg/ml streptomycin (Euroclone, UK).

3.1.3 UM22Bap1$^{+/+}$ and UM22Bap1$^{-/-}$ cells

The human uveal melanoma cell lines UM22Bap1$^{+/+}$ and UM22Bap1$^{-/-}$ were isolated from a patient affected by uveal melanoma (UM) with metastasis, which had a homozygous frameshift deletion in BAP1 gene. UM22Bap1$^{+/+}$ cells were transfected using a retroviral vector with a functional copy of BAP1, while UM22Bap1$^{-/-}$ received an empty vector control sample [107]. UM22Bap1$^{+/+}$ and UM22Bap1$^{-/-}$ were cultured in RPMI-1640 (Cytiva) supplemented with 10% FBS (Euroclone, Pero (MI), Italy), 100 units/ml penicillin, 100 mg/ml streptomycin (Cytiva), and 2 mM L-glutamine (Cytiva).

3.2 Preparation of EV-depleted FBS

During my abroad period, to obtain EV-depleted FBS I tested three slightly different protocols based on different combinations of ultracentrifugation (UC) and heat inactivation (HI). The EV depletion of FBS was performed by ultracentrifugation at 100,000 × g (Type 70 Ti, fixed angle rotor) for 105 min at 4°C. The heat-inactivation was performed by placing FBS in a water bath at 56 ºC for 30 minutes under agitation. The protocol was the same for all conditions except for the moment when the heat inactivation is performed: (a) FBS was ultracentrifuged but not heat-inactivated; (b) FBS was heat-inactivated before UC; (c) FBS was heat-inactivated after EV depletion. After UC, the pellet was discarded, while the supernatant was filtered through a 0.22 µm and then stored at -20°C before use. It was found that performing HI after UC contaminates cell-derived SEVs, thus demonstrating that in EV studies FBS should not be HI or the HI should be performed before UC [108].

3.3 Small extracellular vesicles isolation

3.3.1 CRC cells-derived SEVs

SEVs were isolated from the conditioned culture medium of SW480 and SW620 cells maintained in the presence of EV-depleted FBS. The conditioned medium was collected after a culture period of 24h and then subjected to differential centrifugations followed by ultracentrifugation as previously described [95]. Briefly, the conditioned culture medium was centrifuged for 5 min at 300×g, 15 min at 3,000×g and 30 min at 10,000×g; the supernatant was then ultracentrifuged for 105 min at 100,000×g in a Type 70 Ti, fixed angle rotor.

3.3.2 Plasma-derived SEVs

The results obtained by using SEVs from cell cultures were validated by using SEVs isolated from plasma of CRC patients and healthy donors (Table 1) and from human biopsies (Table 2). Following the manufacturer's instructions, Total Exosome Isolation Kit (Invitrogen) was used for isolating SEVs from 100 µl of plasma samples. Briefly, the plasma was centrifuged for 20 min at 2000× g and 20 min at 10,000× g at room temperature. The supernatant was mixed with 0.5 volume of 1X PBS and vortexed, then a 0.2 volume of Exosome Precipitation Reagent (from plasma) was added to the samples and vortexed again. The samples were incubated at room temperature for 10 minutes and centrifugated for 5 min at 10,000× g at room temperature.

At the end of the isolation procedure, the SEV pellets obtained from both conditioned culture medium and plasma samples were resuspended in no more than 100 µl PBS, the SEV proteins were measured by the Bradford protein assay and SEV pellets were then stored at −80 °C until use. Particle size distribution and concentration were measured as described in the previous paragraph.

TABLE 1 Information about plasma samples from patients (P) with CRC and healthy controls (HS)

Plasma sample	*Sex*	*Age*	*Disease status*	*Diagnosis*	*TNM-stage*	*Grading*
P1	F	48	CRC	ADC	T3N0Mx	2
P2	M	75	CRC	ADC	T3N1aMx	2
P3	M	71	CRC	ADC	T3N0Mx	2
P4	M	74	CRC	ADC	T3N0Mx	2
P5	M	55	CRC	ADC	T3N2bMx	2
HS1	M	57	Absent	-	-	-
HS2	F	44	Absent	-	-	-
HS3	F	26	Absent	-	-	-
HS4	F	35	Absent	-	-	-
HS5	F	39	Absent	-	-	-

CRC: Colorectal Cancer; ADC: Adenocarcinoma

3.3.3 CRC biopsies-derived SEVs

Finally, SEVs were also isolated from CRC biopsies (CRC/B, Table 2) and from the adjacent non-tumoral mucosa (Adjacent Non-CRC biopsies: AdNCRC/B, Table 2) using the protocol established previously by Crescitelli et al. [109] with minor modifications. The tissue pieces were gently sliced into small fragments (1–2 mm) and incubated with collagenase D (Roche, Basel, Switzerland) (2 mg/ml) and DNase I (Roche, Basel, Switzerland) (40 U/ml) dissolved in RPMI plain medium (St Louis, MO, USA) for 30 min at 37°C. After incubation, the samples were passed through a 70 µm filter.

The resulting filtered liquid was centrifuged at 300 x g for 10 minutes, 2,000 × g for 20 minutes and ultracentrifuged at 16,500 × g for 6 minutes (TLA 100.3, k-factor: 404.5, Beckman Coulter, Miami, FL, USA) to remove cells, tissue debris and large EVs. The remaining supernatant was ultracentrifuged at 120,000 x g for 65 minutes (TLA 100.3, k-factor: 55.5, Beckman coulter) to pellet small EVs.

TABLE 2 Information about biopsy samples of patients with CRC

Biopsy	*Sex*	*Age*	*Diagnosis*	*TNM-stage*	*Grading*
NCRC/B1	M	79	ADC	T3bN0Mx	3
CRC/B1					
NCRC/B2	M	58	ADC	T3N2aMx	3
CRC/B2					

CRC/B: Colorectal Cancer biopsy;

AdNCRC/B: Adjacent Non-Colorectal Cancer mucosa biopsy; ADC: Adenocarcinoma

3.3.4 UM cells-derived SEVs

SEVs were isolated from the conditioned media of UM22Bap1$^{+/+}$ and UM22Bap1$^{-/-}$ cell lines as described previously [110]. The conditioned media was collected after 72h and subjected to differential centrifugations. Cells and debris were removed by centrifugations at 300 × g for 10 min and at 2,000 × g for 20 min at 4°C. The supernatant was centrifuged at 16,500 × g for 20 min at 4°C and 118,000 × g for 2.5 h at 4°C to collect SEVs (Type 45 Ti rotor, 38,800 rpm, k-factor 178.6, Beckman Coulter). At the end of the isolation procedure, the SEV pellets obtained from both conditioned culture medium of UM cells and biopsies samples were resuspended in PBS and further purified by a bottom-loaded Iodixanol density cushion (OptiPrepTM, Sigma-Aldrich, St Louis, MO, USA). Briefly, the SEVs were bottom-loaded by mixing 1 ml sample with 3 ml of 60% OptiPrepTM which was placed at the bottom of an ultracentrifuge tube. On top of this, 4 ml of 30% OptiPrepTM and 4 ml of 10% was carefully layered on top. The samples were then centrifuged at 97,000 × g for 2 hours (SW 41 Ti, k-factor: 265.1, Beckman Coulter, Miami, FL, USA). After centrifugation, the visible band containing the purified vesicles was collected from the 10%/30% interface (1.078 g/mL and 1.175 g/ml OptiPrepTM). To remove the contamination from OptiPrepTM, SEVs were further centrifuged at 120,000 x g for 65 minutes (TLA 100.3, k-factor: 55.5, Beckman coulter, Miami, FL, USA). Protein was estimated with the Qubit assay system (Thermo Fisher Scientific, Waltham, MA, USA) following manufacturer's instructions.

3.4 Transmission electron microscopy (TEM)

3.4.1 CRC cells and plasma-derived SEVs

To perform the morphological characterization of isolated sEVs, TEM microscopy analyses were performed in two different labs depending on the origin of the processed samples. For SEVs isolated from conditioned culture medium and plasma samples: SEVs were prepared for electron microscopy studies using negative staining. SEVs suspension of 5µl was deposited onto the carbon-coated EM grids. After washing, the samples were fixed for 5 min in 1% glutaraldehyde and negatively stained with 2% phosphotungstic acid. The grids were viewed in a JEM 1400 Plus electron microscope (Jeol, Japan) operating at 80 kV equipped with a CCD camera.

3.4.2 CRC biopsies-derived SEVs

For SEVs isolated from tissue samples: investigation of SEVs by negative staining was performed as previously described [109]. Briefly, 2.3 µg of SEVs was placed onto glow discharged 200-mesh formvar/ carbon copper grids (Electron Microscopy Sciences, Hatfield Township, PA). After two washes in H2O, SEVs were fixed in 2.5% glutaraldehyde. After two further washes in H2O, the samples were stained with 2% uranyl acetate for 1.5 min. Negative-stained samples were examined on a digitized Talos L120C electron microscope (Thermo Fisher Scientific) at 120 kV with a CCD camera.

3.5 Scanning electron microscope (SEM)

For scanning electron microscope (SEM) analysis liver spheroids were collected at the end of the experiment and washed two times with PBS. After washing, liver spheroids were fixed with 2.5% glutaraldehyde and stored in 70% ethanol. SEM analyses, spheroids slicing, and haematoxylin/eosin staining were performed by Prof. Maria Cristina Guerrera at the University of Messina.

3.6 Treatment of hepatocytes

To analyze the effects induced by the CRC_sEVs on hepatocytes, the following protocol of treatment was applied. After reaching sub-confluence, THLE-2 cells were treated for the indicated time points with about 1.5*E10 particles of SEVs derived from CRC cells corresponding to 20 µg/ml, the dose we found effective in our previous study [90, 95]. Thus, the same number of particles/ml was used for treating the THLE-2 cells with SEVs from the plasma of healthy subjects and CRC patients, from CRC and adjacent non-CRC biopsies and UM cells. On day 5, liver spheroids were treated for the indicated time points with about 1.5*E10 particles of SEVs derived from SW480 cells.

After treatment, THLE-2 cells and liver spheroids were harvested for real-time quantitative PCR, Western Blot, or immunofluorescence analysis by confocal microscopy.

3.7 Western blot

THLE-2 cells, SEVs (from cells or plasma), or liver spheroids were lysed using RIPA buffer with protease inhibitor cocktail (Thermo Fisher Scientific, Waltham, MA, USA) (1:100 dilution) for 1h and 30 min on ice and then centrifuged at 18,800 × g for 15 min at 4 °C.

The extracted proteins were measured using the Bradford protein assay (Pierce, Rockford, IL, USA). Proteins were separated on Bolt 4-12% Bis-Tris Plus precast polyacrylamide gels (Invitrogen by Thermo Fisher Scientific, Waltham, MA, USA) under reducing conditions, except for TGFβ1 analysis. Following electrophoresis, proteins were transferred to a nitrocellulose blotting membrane (Amersham Protran Premium 0.45 µm NC by GE HealthCare Life Science, Little Chalfont, Buckinghamshire, UK), blocked in 1% BSA and incubated with primary antibodies overnight at 4°C. Primary antibodies used for sEV characterization were: anti-CD81 (1:1000 dilution; Santa Cruz Biotechnology, Dallas, TX, USA), anti-HSC70 (1:1000 dilution; Santa Cruz Biotechnology, Dallas, TX, USA), anti-Calnexin (1:1000; Santa Cruz Biotechnology, Dallas, TX, USA), anti-cytochrome c (1:1000; Cell Signaling Technology, Danvers, MA, USA); the primary antibody anti-TGFβ1 antibody (1:300 dilution; Santa Cruz Biotechnology, Dallas, TX, USA) was used to assess the presence of TGFβ1 in CRC_sEVs; primary antibodies used for investigating the modulation of mediators of the TGFβ1 signalling and the related targets were: anti-SMAD 2/3 (1:300 dilution; Cell Signaling Technology, Danvers, MA, USA), anti-pSMAD 2/3 (1:300 dilution; Cell Signaling Technology, Danvers, MA, USA), anti-SNAIL (1:300 dilution; Cell Signaling Technology, Danvers, MA, USA), anti-SLUG (1:300 dilution; Cell Signaling Technology, Danvers, MA, USA), anti-vimentin (1:300 dilution; Cell Signaling Technology, Danvers, MA, USA), anti-αSMA (1:300 dilution; Cell Signaling Technology, Danvers, MA, USA), anti-CK8/18 (1:300 dilution; Cell Signaling Technology, Danvers, MA, USA), anti-E-Cadherin (1:300 dilution; Cell Signaling), and anti-HNF4 (1:300 dilution; Santa Cruz Biotechnology, Dallas, TX, USA). Anti-β actin (1:1000 dilution; Santa Cruz Biotechnology, Dallas, Tx, USA), anti-GAPDH (1:1000 dilution; Santa Cruz Biotechnology, Dallas, TX, USA), and anti-Tubulin (1:1000 dilution; Santa Cruz Biotechnology, Dallas, TX, USA) were employed to detect proteins used as loading control. After washing with Tris-buffered saline +Tween 20 (TBS/T) three times, the membrane was incubated with horseradish peroxidase (HRP)-conjugated goat anti-rabbit or anti-mouse secondary antibodies (1:1000 dilution; Thermo Fisher Scientific, Waltham, MA, USA) at room temperature for 1 h.

The protein bands were visualized by enhanced chemiluminescence (ECL™ Prime Western Blotting System Cytiva RPN2232) by using the Chemidoc imaging system (Bio-Rad, Milan, Italy). GAPDH, Actin, and tubulin were used as the loading controls. Densitometric analysis of the Western blot was performed by using ImageJ software.

3.8 Cytotoxicity assay

To evaluate if SEVs can have a toxic effect on hepatocytes growth, the CellTox™ Green Cytotoxicity Assay was performed (G8741, Promega, Madison, WI, USA). THLE-2 cells were cultured in triplicate at 5×10^3 cells/well into white-walled, opaque 96 well plates; 24h post-seeding, cells were treated for 24 and 48h with approximately 1.5*E10 particles of SW480_SEVs, SW620_DEVs, CRC_P/DEVs (P1-5) and HS/DEVs (HS1-5). Changes in membrane integrity that occur as a result of cell death were measured as relative fluorescence unit (RFU) by Glomax (Promega, Madison, WI, USA).

3.9 Real-Time PCR

Total RNA was extracted using illustra™ RNA spin mini-RNA isolation Kit (GE Healthcare, Little Chalfont, Buckinghamshire, UK). The RNA was reverse transcribed to cDNA using the High-Capacity cDNA Reverse Transcription kit (Applied Biosystems, Foster City, CA, USA). Then, the cDNA was subjected to quantitative real-time reverse transcriptase-polymerase chain reaction (RT-PCR) analysis. The sequences of the used primers are reported in the Table 3. Real-time PCR was performed using Step One™ Real time PCR System Thermal Cycling Block (Applied Biosystems, Waltham, MA, USA) in a 20 µl reaction containing 300 nM of each primer, 2 µl template cDNA, 18 µl 2X SYBR Green I Master Mix. The PCR was run at 95°C for 20 sec followed by 40 cycles of 95°C for 3 sec and 60°C for 30 sec. GAPDH was used as the endogenous control. Relative changes in gene expression between control and treated samples were determined using the ΔΔCt method.

TABLE 3 Primers used in RT-PCR

Primers	*Forward*	*Reverse*
GAPDH	ATGGGGAAGGTGAAGGTCG	GGGTCATTGATGGCAACAATAT
ALB	GAGACCAGAGGTTGATGTGATG	GCCATCATCTTCTTTGACCCA
APOE	TGGCACTGGGTCGCTTTTGGG	TCATGGTCTCGTCCATCAGCGC
CYP3A4	AAGTCGCCTCGAAGATACACA	AAGGAGAGAACACTGCTCGTG

3.10 Enzyme-Linked ImmunoSorbent Assay (ELISA) of albumin

The amount of albumin in the culture medium of THLE-2 cells and liver spheroids treated with CRC cells-derived SEVs was determined by human albumin ELISA kit (Abcam, Cambridge, UK). The ELISA assay was performed according to the manufacturer's instructions.

3.11 Confocal fluorescent microscopy

At the end of the treatment, THLE-2 cells and liver spheroids were fixed by the addition of PFA 4%, permeabilized with TritonX-100, and incubated at room temperature with primary antibodies: anti-HNF4 (1:50 dilution; Santa Cruz Biotechnology, Dallas, TX, USA), anti-CK8/18 (1:50 dilution; Cell Signaling Technology, Danvers, MA, USA), anti-vimentin (1:50 dilution; Cell Signaling Technology, Danvers, MA, USA), anti-Ecadherin (1:50 dilution; Cell Signaling Technology, Danvers, MA, USA), and anti-Fibronectin (1:50 dilution; Cell Signaling Technology, Danvers, MA, USA). Unbound primary antibody was then removed, and cells were washed with ice-cold PBS and incubated with DyLight 488 or Dylight 594 secondary antibody (1:500 dilution; Thermo Fisher Scientific, Waltham, MA, USA). Unbound secondary antibody was aspirated off, cells were washed with ice-cold PBS, and nuclei were stained with Hoechst (Molecular Probes, Life Technologies, Carlsbad, CA, USA). In some cases, cells were stained with Actin Green (Thermo-fisher, Waltham, MA, USA) (1:125 dilution) to detect F-actin. Finally, the samples were analyzed by confocal fluorescence microscopy (Nikon A1).

3.12 dSTORM characterization

Direct stochastic optical reconstruction microscopy (dSTORM) is an emergent single-molecule super-resolution imaging technique with a practical resolution limit of 20 nm used extensively to image and characterize the anatomy, organisation, and biomechanical properties of subcellular structures as EVs [111]. SEVs prepared from SW480 and SW620 cells (1.8×10^7 and 3.5×10^7 particles, respectively) were immunolabeled overnight at 4°C using a cocktail of fluorescently labeled antibodies against CD9 (Atto488 mouse anti-human monoclonal; FL-REA-EV-CD9-Atto488, ONI), CD63 (Cy3BTM mouse anti-human monoclonal; FL-REA-EV-CD63-Cy3b, ONI), and TGFβ1 (Alexa Fluor®647 mouse anti-human monoclonal; IC10502R, R&D Systems). They were then loaded and captured on the surface of a PEG-Biotin functionalized microfluidic chip included in the EasyVisi Single-Extracellular Vesicle Characterization kit from ONI (beta version 1.0, Oxford Nanoimaging, UK). Surface preparation, removal of unbound antibodies, and crosslinking of EVs to the chip surface, including all wash steps, were done using the EasyVisi kit and automated using a Roboflow microfluidic sample preparation platform (ONI). Direct stochastic optical reconstruction microscopy (dSTORM) imaging was then performed after freshly prepared BCubed STORM-imaging buffer (ONI) was added to each lane on the microfluidics chip. Single-molecule fluorescence data consisting of 2000 frames per channel, was sequentially acquired using the Nanoimager S Mark II with laser power set to 45, 50, and 50% for the 640, 560, and 488 lasers, respectively.

An Olympus 1.4NA 100x oil immersion super apochromatic objective was used with angle of illumination set to 52.5°. Channel mapping was calibrated at the start of the imaging session using 0.1 µm Tetraspeck beads (#T7279, Thermo Fisher Scientific). Data was processed on NimOS software (version 1.18; ONI). To identify EV subpopulations that express one, two, or three markers, single-molecule data was analyzed using algorithms developed by ONI via their online localization microscopy data analysis platform beta-released named CODI (https://alto.codi.bio/, releases 0.16.0 to 0.14.1; March 9th to April 28th, 2021). The analysis workflow of SEV data included filtering, drift correction, and subsequent clustering using hierarchical density-based clustering algorithms for single-EV analysis.

3.13 Trypsin digestion of CRC_SEVs and TGFβ1 ELISA assay

To assess the SEV surface localization of TGFβ1, approximately 200 µg of SW480_SEVs and SW620_SEVs were resuspended in a final volume of 0.5 ml of PBS with 0.125% trypsin (Corning, Manassas, VA) and incubated at 37°C for 15 minutes under agitation [112, 113]. At the end of the reaction, the sEVs were diluted in 40 ml PBS and subjected to ultracentrifugation for 105 min at 100,000× g in a Type 70 Ti fixed angle rotor. Finally, the pellet was resuspended in PBS and analyzed by NTA to assess the integrity of SEVs after treatment with trypsin and by ELISA to verify TGFβ1 removal. Untreated SW480_SEVs and SW620_SEVs were used as a control.

The presence of TGFβ1 in trypsin-treated and untreated SW480_SEVs and SW620_SEVs was determined by using a TGFβ1-specific ELISA kit (Sigma-Aldrich, USA). The assay was performed using the same number of particles determined by NTA. The ELISA assay was then performed according to the manufacturer's instructions.

3.14 CellTiter-Glo® 3D Cell Viability Assay

To test the viability of liver spheroids following the treatment with SW480_SEVs, we performed CellTiter-Glo® 3D Cell Viability Assay. Briefly, liver spheroids were treated with SW480_SEVs for 48h, then they were transferred in opaque-walled 96 well plates and we added 100 µl of CellTiter-Glo® 3D Reagent. The plate was incubated for 5 min under agitation to induce cell lysis, then for additional 25 min to stabilize the luminescent signal. The luminescence was recorded using Glomax.

3.15 Lactate Dehydrogenase (LDH) cytotoxic assay

The conditioned media of liver spheroids was collected after 48 h of treatment with SW480_SEVs and the Lactate Dehydrogenase (LDH) assay was performed according to the instructions of the LDH-Glo™ Cytotoxicity Assay kit (Promega, Madison, WI, USA).

Briefly, 50 µL of medium (diluted 1:100 in LDH Storage Buffer) were transferred into a 96-well plate in duplicate wells, then 50 µL of LDH Detection Reagent were added to each well and incubated for 60 minutes at room temperature. Finally, the luminescence was recorded using Glomax. The cytotoxicity was calculated using the following formula: (LDH in treated cells × 1) / (LDH in control cells)

3.16 Statistical Analysis

Statistical analysis was performed using GraphPad Prism software 9.5.1 (GraphPad software, Inc., La Jolla, CA). Values reported in all graphs are the mean ± standard deviation (SD) of three replicates, unless otherwise stated. The statistical significance of the differences was analyzed using a two-tailed Student's t-test. A p-value ≤0.05 was considered significant.

3.17 Ethics statement

Human plasma collections were approved by the Institutional Ethics Committee Catania 2 - ARNAS Garibaldi Hospital, Catania, Italy (20/07/2020; 436/C.E.) and by the Institutional Ethics Committee Palermo 1 - Policlinic University Hospital "Paolo Giaccone", Palermo, Italy (23/09/2020; 8/2020); healthy donors (n=5), CRC patients without metastasis (n=5). CRC tissue samples (n=2) and adjacent non-CRC mucosa (n=2) were collected from patients undergoing surgical tumor resection at the Department of Surgery at Sahlgrenska University Hospital, Gothenburg, Sweden, in accordance with the rules and regulations of the Central Ethical Review Board of Gothenburg (Dnr 995-16 and 2019-04873). All enrolled individuals provided informed consent according to the protocol approved by the referent institutional review board.

4. Results

4.1 Characterization of SEVs isolated from CRC cell lines

SEVs from culture supernatants of the human CRC cell lines SW480 and SW620 were isolated and collected as described in the Methods section and characterized. The NTA showed that SEVs isolated from SW480 cells are more heterogeneous regarding size than vesicles derived from SW620, but the two populations have equivalent concentration of 1.5×10^8/ml (Fig. 13 A). Regarding the observed size, we found that both SW480_SEVs and SW620_SEVs have an average size close to what was previously described [80], as confirmed by the modal size, although the presence of multiple peaks in the graph highlight that the size of isolated SEVs was not completely homogeneous (Fig. 13 A). Next, the TEM images reported in Fig. 13 B showed particles with the typical spherical structure mainly ranging between 120-150 nm in accordance with the classical SEV size distribution, confirming the NTA results. Finally, SEVs derived from CRC cell lines were characterized by protein analysis. Typical EV markers (HSC70 and CD81) were positive in SEVs, while the absence of Calnexin and Cytochrome C indicated no contamination by endoplasmic reticulum and mitochondrial proteins (Fig. 13 C).

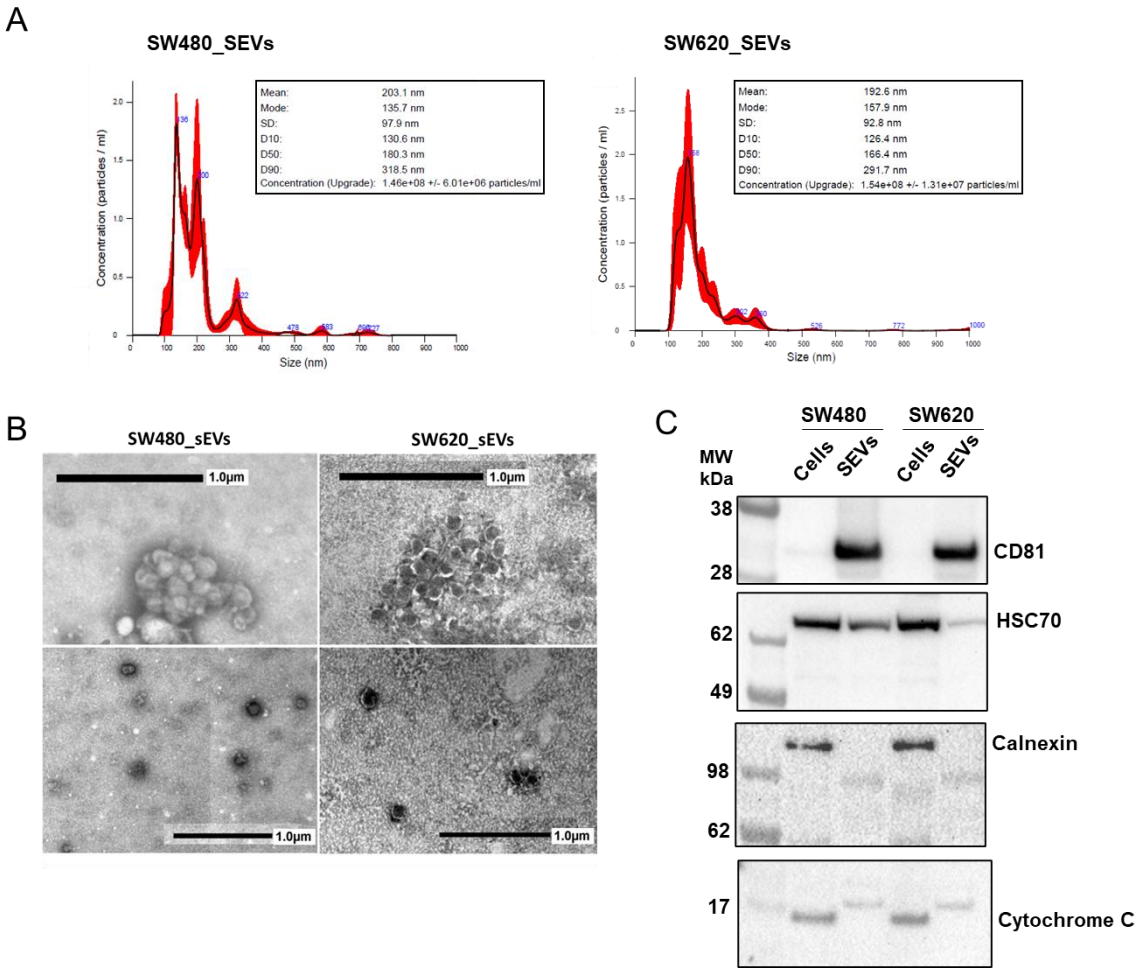

FIGURE 13 Characterization of SEVs isolated from CRC cell conditioned media by ultracentrifugation. (A) NanoSight NTA analysis of the sizes of SW480_SEVs and SW620_SEVs. (B) Representative TEM micrographs of SEVs isolated from CRC cell culture medium in which clusters (upper panel) and single vesicles (lower panel) are showed. (C) SEVs were compared to whole cell lysates by Western Blot. Membranes were probed using antibodies against CD81, HSC70, Calnexin, and Cytochrome C.

4.2 CRC_SEVs modulate the expression of hepatocytes markers

After ensuring that CRC_SEVs did not have toxic effects on heps (Fig. 14 A), we analyzed the expression levels of some functional hepatocyte-specific genes such as albumin (ALBU), apolipoprotein E (APOE), and cytochrome P450 3A4 (CYP3A4) [114, 115], following the treatment with CRC_SEVs. We observed that both SW480_SEVs and SW620_SEVs after 24h significantly inhibited the expression of the three genes, and this effect was stronger after 48h (Fig. 14 B). Moreover, for both SEV types, the downregulation of ALBU after 24h of treatment was also confirmed at the protein level by ELISA (Fig. 14 C). To assess the ability of CRC_SEVs to alter the key phenotypic characteristics of heps we also analyzed by confocal microscopy the expression and the localization of the Hepatocyte Nuclear Factor 4 (HNF-4), central regulator of hepatocyte differentiation and function [116]. According with the data on ALBU, APOE and CYP3A4, we found that the treatment for 24h with CRC_SEVs induced a clear reduction of HNF-4 correlating with its low nuclear localization in comparison to no-treated cells (Fig. 14 D). It was interesting to observe that the negative modulations at gene/protein levels corresponded to evident morphological changes. As it is observable in the representative micrographs in Fig. 14 E, we observed that when treated with CRC_SEVs, the heps formed a monolayer that lost its regular and well-arranged structure and was characterized by the appearance of spaces between cells (yellow arrows).

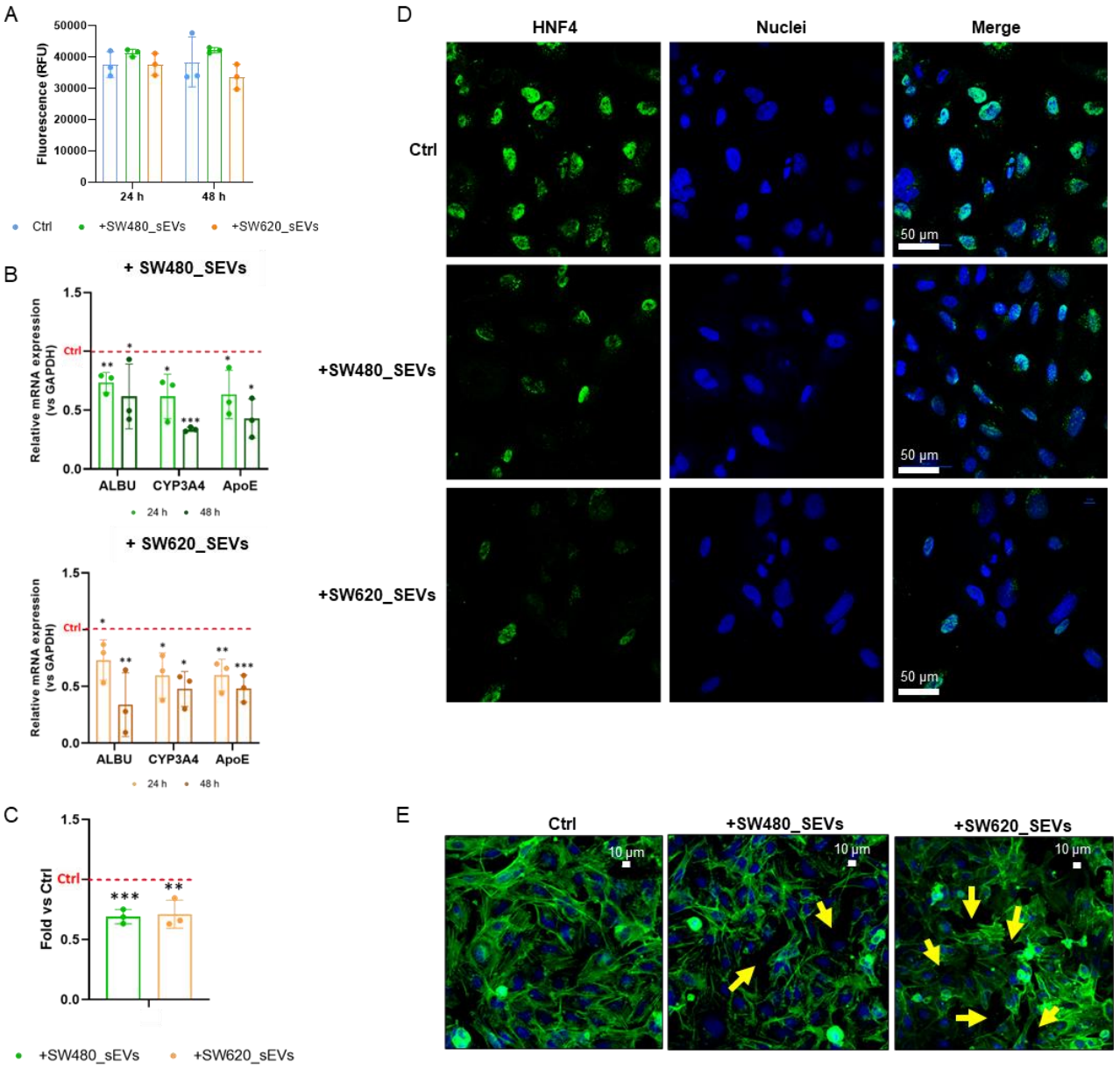

FIGURE 14 CRC_SEVs alter the functional properties and morphology of heps. (A) CellTox assay showed that treatment for 24 and 48 h with CRC_SEVs did not alter the viability of THLE-2 cells (RFU: relative fluorescence units). (B) Gene expression levels of ALBU, CYP3A4, and APOE were measured in THLE-2 cells treated with CRC_SEVs. (C) ELISA assay of ALBU released in the conditioned medium of THLE-2 cells treated with CRC_SEVs for 24h. In all reported graphs, the asterisks indicate significant differences vs untreated control cells (Ctrl) (*p<0.05; **p<0.01; ***p<0.01). (D) Fluorescent confocal microscope images showing HNF4 expression and localization in THLE-2 cells treated for 24h with CRC_SEVs; (E) Fluorescent confocal microscope images showing the morphological changes of THLE-2 cells induced by treatment with CRC_SEVs for 24h; Actin Green (green) was used to stain actin fibers; Hoechst (blue) was used to stain the nuclei; the yellow arrows indicate the CRC_SEV-induced holes in the THLE-2 cells monolayer. Ctrl: untreated control cells.

To understand if the morphological changes observed in the CRC_SEV-treated heps, were associated with modulation of structural proteins, we evaluated by confocal microscopy the expression levels of the cytoskeletal proteins vimentin and CK8/18.

The representative micrographs reported in Fig. 15 showed that 24h treatment with CRC_SEVs induced a simultaneous increase in vimentin and decrease in CK8/18 in comparison to the control, leading us to hypothesize the ability of CRC_SEVs to initiate heps towards the EMT process.

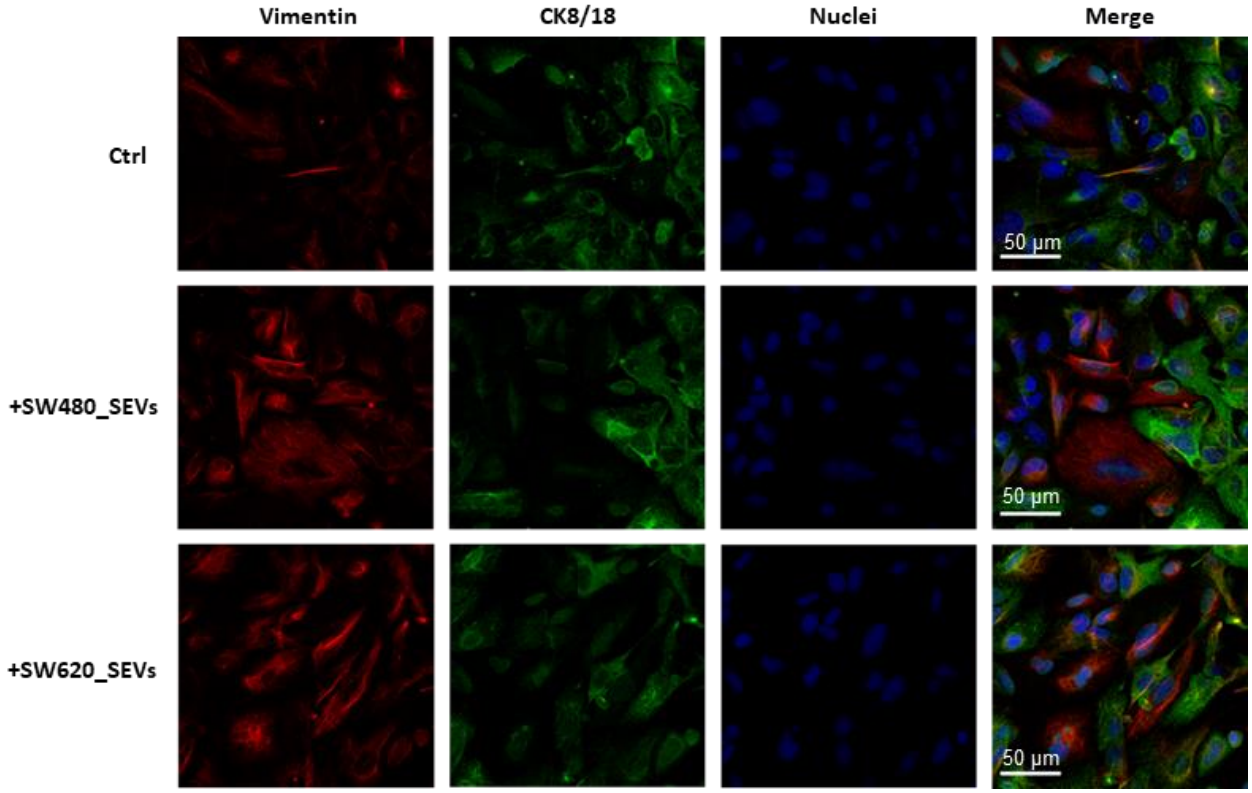

FIGURE 15 Confocal microscopy analysis of vimentin (red) and CK8/18 (green) in THLE-2 cells treated with CRC_sEVs for 24h; nuclei are in blue. Untreated cells are indicated as a control (Ctrl).

4.3 CRC_SEVs carry TGFβ1

The inhibition of the ALBU and HNF4 expression as well as the observed morphological changes can be ascribed to TGFβ1 activity [117, 118] known to be carried by EVs including those released by CRC cells [112, 119]. Based on these considerations, we investigated the presence of this cytokine in SEVs isolated from both SW480 and SW620 cells. As shown in Fig. 16 A, western blot assays showed that CRC_SEVs were enriched in TGFβ1 compared with the cells, indicating that colorectal cancer cells secrete TGFβ1 into the surrounding environment through SEVs. According to data from the literature [112], we found that SEV from SW480 and SW620 cells, in addition to the monomer, also carried the latent form of TGFβ1 (Fig. 16 A). Furthermore, dSTORM imaging revealed that TGFβ1 is located on the surface of the SEVs, as demonstrated by its colocalization with CD9 and CD81 (Fig. 16 B). Interestingly, this analysis also highlighted that both SW480 and SW620 cells release a heterogeneous population of SEVs, as already described in other cell models [120].

As reported in the graphs in Fig. 16 B, we found the following seven SEV phenotypes for each cell line: $CD9^+/CD63^+/TGF\beta1^+$ (28.6% and 24%, respectively, for SW480 and SW620 cells), $CD9^+/CD63^+$ (54.3% and 60%, respectively, for SW480 and SW620 cells), $CD9^+/TGF\beta1^+$ (2% and 1.6%, respectively, for SW480 and SW620 cells), $CD63^+/TGF\beta1^+$ (3% and 2%, respectively, for SW480 and SW620 cells), $CD9^+$ (4.5% and 3.3%, respectively, for SW480 and SW620 cells), $CD63^+$ (5.6% and 8.2%, respectively, for SW480 and SW620 cells), and $TGF\beta1^+$ (2% and 0.5%, respectively, for SW480 and SW620 cells). These data indicated that in total, approximately 35% of SEVs released by SW480 cells and 30% of those released by SW620 cells carry TGFβ1.

To confirm the SEV surface localization of TGFβ1, we verified the effects of treatment with trypsin on the TGFβ1/SEV association. Thus, CRC_SEVs were subjected to trypsin digestion and the presence of TGFβ1 was detected by an ELISA assay. As shown in Fig. 16 C, a significant decrease in TGFβ1 was observed in trypsin treated SEVs in comparison to untreated SEVs.

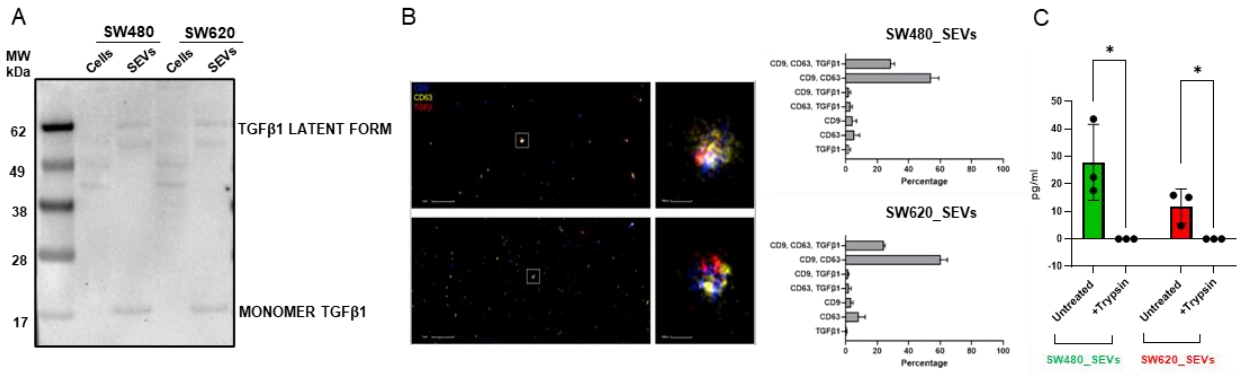

FIGURE 16 CRC_SEVs carry TGFβ1. (A) Western Blot analysis of TGFβ1 in SW480 and SW620 cells and derived SEVs. (B) dSTORM imaging of SW480_ and SW620_ SEVs. The graphs on the right report the ratios of the number of each sEV group to the total number of counted sEVs expressed as a percentage. (C) ELISA assay showing the effect of the trypsin treatment on the presence of TGFβ1 in CRC_SEVs.

To corroborate our investigations, in addition to SEVs obtained by the in vitro systems, THLE-2 cells were treated with SEVs isolated from the plasma of CRC patients (CRC_P/SEVs, n=5) and healthy subjects (HS/SEVs, n=5). These *ex vivo* SEVs were characterized by TEM and NTA, of which respectively in Fig. 17 A and B representative images (relative to the SEVs isolated from sample P2 - Table 1) are reported. Moreover, as shown in Fig. 17 C all SEV samples obtained by plasma of both CRC patients (P1-5) and healthy subjects (HS1-5) were characterized for the presence of EV markers (CD81 and Alix) and for the absence of proteins expected to be underrepresented in EVs (Calnexin and Cytochrome C). Finally, Western Blot assays showed an appreciable difference in the amount of the detected latent form of TGFβ1 between CRC_P/SEVs and HS/SEVs (Fig. 17 D).

It is important to emphasize that since we received plasma samples from CRC patients and healthy subjects at different times, Western blot assays were performed independently. Thus, we paid much attention to making sure to have the same experimental conditions for a proper comparison of the obtained results. Thus, to detect TGFβ1 the same protein amount (50 μg) of each sample was loaded, and both membranes were exposed for 1 min. The non-cytotoxicity of the *ex vivo* SEVs on heps was assessed by the CellTox assay (Fig. 17 E-F)

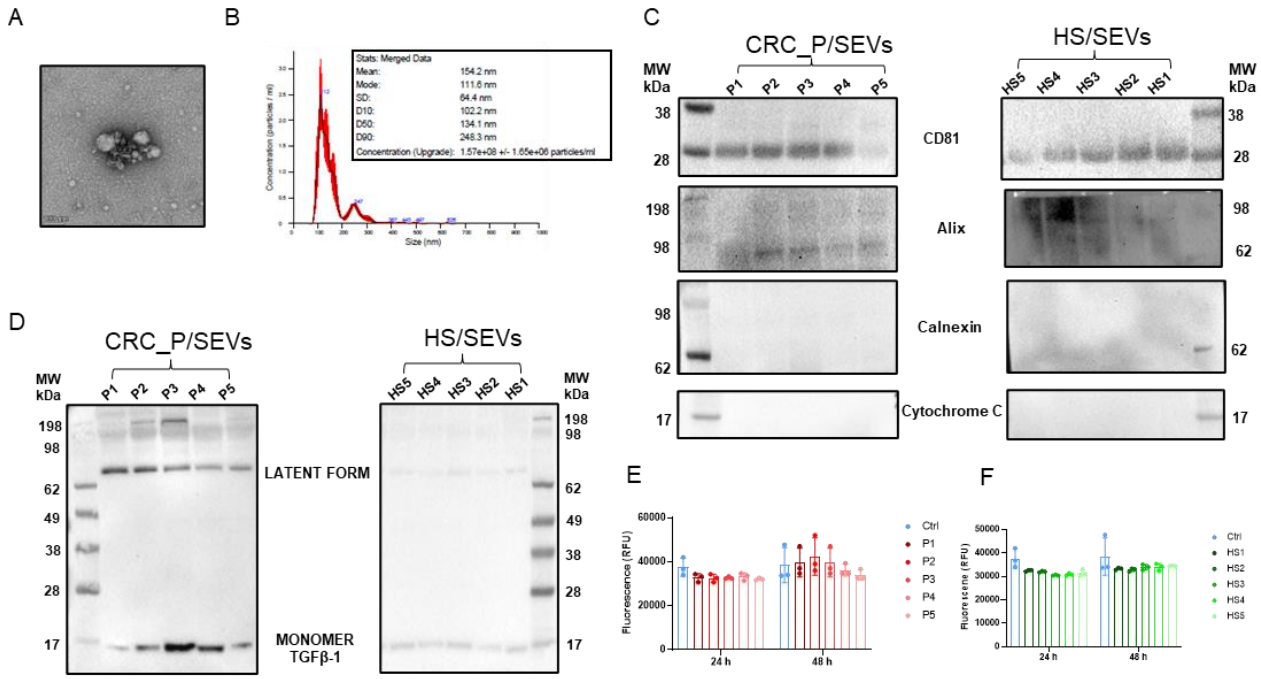

FIGURE 17 Characterization of SEVs isolated from plasma of CRC patients (CRC_P/SEVs) and healthy subjects (HS/SEVs). (A) Representative TEM micrograph and (B) NTA of SEVs isolated from a CRC patient plasma. (C) Western Blot analysis of EVs markers (CD81 and Alix) and of proteins expected to be underrepresented in EVs (Calnexin and Cytochrome C). (D) Western Blot analysis of TGFβ1 in CRC_P/SEVs and HS/SEVs. CellTox assay showed that treatment for 24 and 48h with (E) CRC_P/SEVs and (F) HS/SEVs did not alter the viability THLE-2 cells (RFU: relative fluorescence units).

4.4 CRC_SEVs modulate the expression of EMT markers in hepatocytes

Next, to further validate the biological function of TGFβ1/SEVs, we investigated the signaling pathways activated in CRC_SEV-treated heps. TGFβ1 activates a canonical signalling pathway mediated by SMAD [39]. According to the timing reported in a recent paper by Lötvall's group [112], we found an increase in phospho-SMAD2/3 levels in heps after 1h of treatment with CRC_SEVs (Fig. 18 A), suggesting their ability to activate the canonical TGFβ1 signaling pathway.

Since several studies have described the roles of TGFβ1-activated SMADs in EMT induction [121], our further analyses were focused on TGFβ1/SMAD signalling target genes, including the transcription factors SNAIL and SLUG, which in turn induced the expression of mesenchymal genes (such as vimentin and α-SMA) and the repression of epithelial marker genes (such as E-cadherin and CK8/18) [40, 122]. Western Blot analyses showed that CRC_SEVs elicited in hepatocytes the effects due to the activation of the TGF-β1/SMAD signaling pathway with different time courses for the different analyzed target genes. As reported in Fig. 18 B, the significantly and early upregulated targets were the transcription factors SNAIL (after 6h) and SLUG (after 12h). Moreover, the mesenchymal marker vimentin started to be significantly modulated from 6h, according to data in the literature describing it as an early target gene of the TGFβ1/SMAD signalling pathway [123]. The modulation of vimentin was then appreciable until 48h, when we found that α-SMA was also significantly increased (Fig. 18 C). Finally, a significant repression of the epithelial markers CK8/18 and E-cadherin was detectable after 48h of CRC_SEV treatment (Fig. 18 D). Together, these findings suggest that CRC_SEVs elicited the activation of TGFβ1/SMAD signalling in heps associated with the expression of early and late EMT markers.

According to what we observed with SEVs isolated from SW480 and SW620 cells, we found that SEVs isolated from plasma of CRC patients (CRC_P/SEVs) were able to activate the expression of the EMT transcription factors SNAIL and SLUG as well as vimentin. In detail, the results reported in Fig. 18 E show that CRC_P/SEVs, but not SEVs isolated from plasma of CRC patients (HS/SEVs), induced the upregulation of SNAIL, SLUG and vimentin after 6h of treatment in heps. As specified above, since the Western Blot assays of CRC_P/SEV- and HS/SEV-treated heps were also performed separately, we paid attention to loading the same protein concentration and fixing the same exposure time for protein detection.

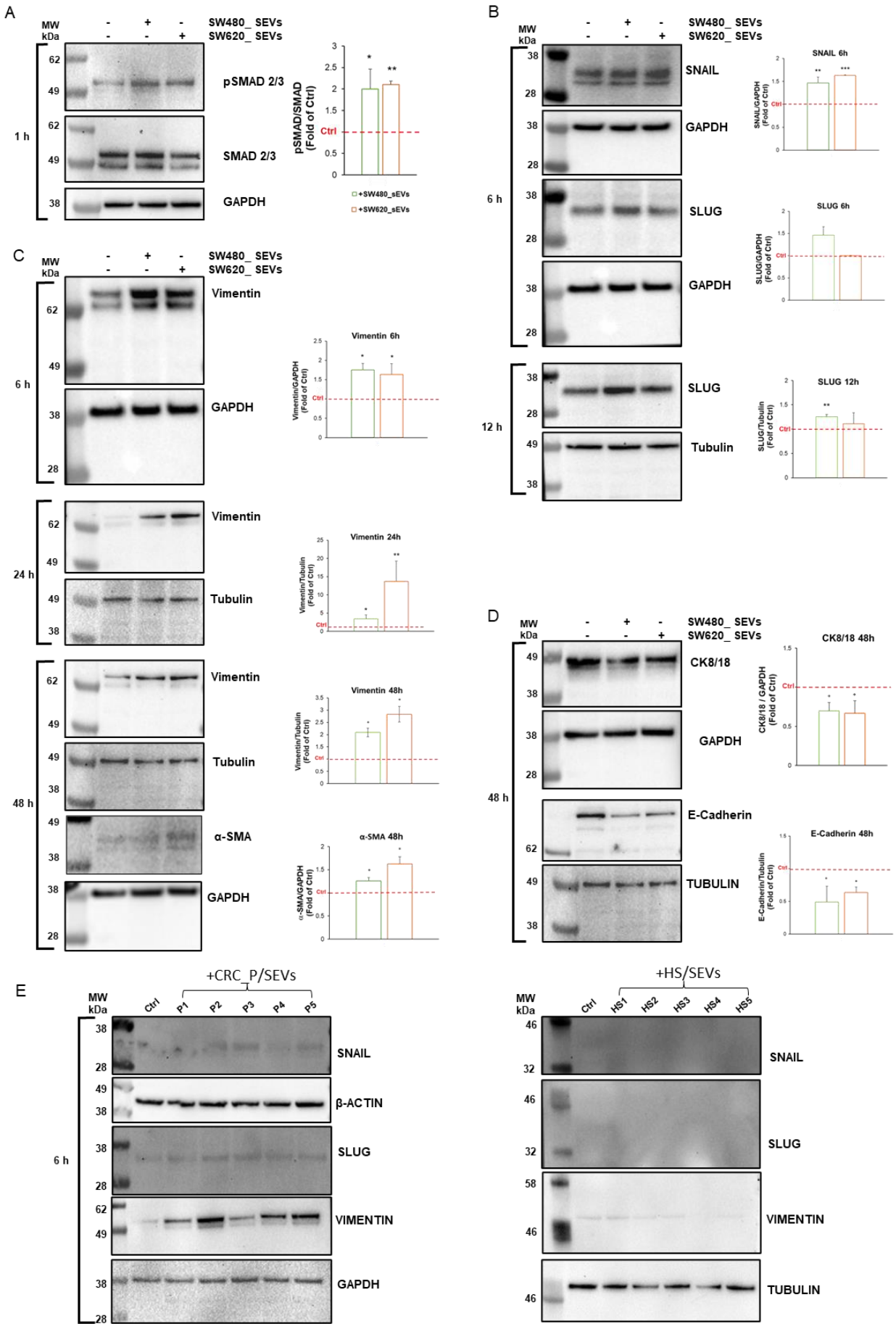
A
MW kDa
SW480_ SEVs
SW620_ SEVs
1 h
pSMAD 2/3
SMAD 2/3
GAPDH
pSMAD/SMAD (Fold of Ctrl)
Ctrl
+SW480_sEVs
+SW620_sEVs
B
6 h
SNAIL
GAPDH
SLUG
SNAIL 6h
SLUG 6h
12 h
SLUG 12h
Tubulin
C
6 h
Vimentin
Vimentin 6h
24 h
Vimentin 24h
48 h
Tubulin
α-SMA
Vimentin 48h
α-SMA 48h
D
CK8/18
CK8/18 48h
E-Cadherin
TUBULIN
E-Cadherin 48h
E
+CRC_P/SEVs
Ctrl
P1
P2
P3
P4
P5
β-ACTIN
VIMENTIN
+HS/SEVs
HS1
HS2
HS3
HS4
HS5

FIGURE 18 CRC_SEVs induce the modulation of TGF-β/SMAD targets associated with EMT in heps. Western Blot assay was performed to verify the ability of SW480_ and SW620_SEVs to modulate in THLE-2 cells (A) the SMAD 2/3 phosphorylation, (B) the expression of SNAIL and SLUG, and of (C) mesenchymal and (D) epithelial markers. Each Western Blot is associated with the correspondent densitometric analysis where the reported values are the mean of at least 2 independent experiments (±SD) of the protein normalized vs loading control (Tubulin or GAPDH). (E) Western Blot analyses of SNAIL, SLUG, and vimentin in THLE-2 cells treated with CRC_P/SEVs and HS/SEVs; Ctrl: untreated control cells. *p≤0.05; **p≤0.01.

Interestingly, we found that the treatment of heps for 24h with SEVs isolated from CRC biopsy (a representative TEM image of these SEVs is reported in Fig. 19 A), induced a concurrent increase in vimentin and a decrease in CK8/18 expression, unlike SEVs isolated from the biopsy of the corresponding non-CRC mucosa (Fig. 19 B).

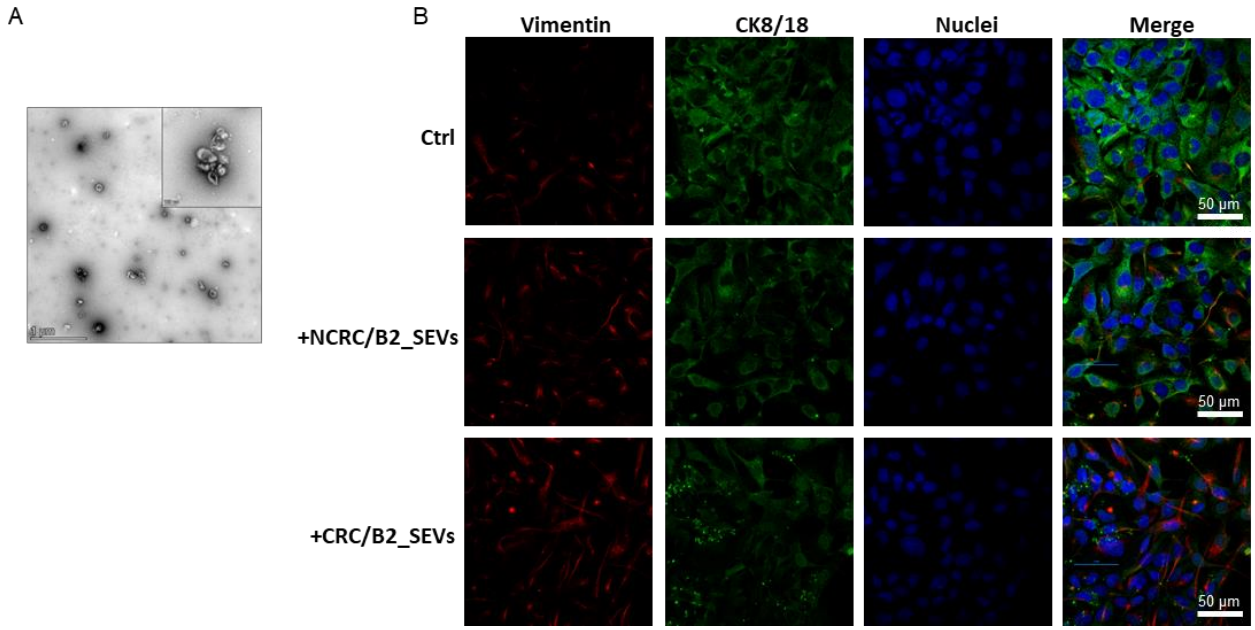

FIGURE 19 SEVs isolated from CRC biopsies modulate the expression of mesenchymal and epithelial markers in hepatocytes. (A) Representative TEM micrograph of SEVs isolated from CRC biopsy (CRC/B1 in Table 2). Scale bars: 1 µm and 100 nm. (B) Confocal microscopy analysis of vimentin (red) and CK8/18 (green) in hepatocytes treated with SEVs isolated from a CRC biopsy (CRC/B2 in Table 2; CRC/B2_SEVs) and from the corresponding non-CRC mucosa (NCRC/B2 in Table 2; NCRC/B2_sEVs) for 24h.; nuclei are in blue. Untreated cells are indicated as control (Ctrl). Scale bars: 50 µm.

All these data were published in the journal Cancer Cell International [124].

4.5 Isolation and characterization of SEVs from uveal melanoma cells

During my abroad period at the University of Gothenburg (Sweden), I focused on the effects of uveal melanoma-derived SEVs on liver parenchyma because liver is the main metastatic site in UM patients [125]. Uveal melanoma (UM) is rare cancer originating from the melanocytes in the uveal tract within the eye [126]. Fifty percent of UM patients will develop metastatic disease, and interestingly 90% of these patients specifically show liver metastases [125] ; the prognosis of patients with metastatic UM is highly dependent on the progression of the disease in the liver [127]. Recently, liver-directed therapies have been developed in an attempt to cure or stabilize liver metastases [13]. Among these therapies, isolated hepatic perfusion (IHP) with melphalan, a known anti-cancer chemotherapy drug [128], consists of the connection of the liver with a heart–lung machine to perfuse the liver with a high dose of chemotherapy under hyperthermia [129]. In 1994, percutaneous hepatic perfusion (PHP) was performed for the first time [130]. The principle of PHP is the same of IHP, however, it is less invasive thus reducing morbidity and mortality related to the open procedure and it reduces the time of the procedure [13].
However, the reasons why the liver is the almost exclusively metastatic site are still unknown and the role of UM-derived SEVs in initiating liver metastasis has not been elucidated yet.
Previously work done by Olofsson Bagge's group described recurrent mutations of the cells in UM and found that BAP1 mutation is correlated with liver metastasis [107]. BAP1 is a multifunctional tumor suppressor gene involved in chromatin remodeling, DNA damage response, cell cycle control, regulation of cell death, and the immune response [131]. They established two UM cell lines, UM22Bap1$^{+/+}$ and UM22Bap1$^{-/-}$, were isolated from a patient affected by UM with metastasis, which had a homozygous frameshift deletion in BAP1 gene [107]. We isolated and characterized UM cells-derived SEVs through TEM to investigate the size of SEVs. TEM images (Fig. 20 A) showed a high background probably due to protein contaminants, thus we performed iodixanol density gradient ultracentrifugation to separate EVs from protein contaminants. The TEM image (Fig. 20 B) shows that the background is minimal and the vesicles were more concentrated. Moreover, we analyzed the presence of canonical EV markers by western blot. While heat shock protein 90 (GRP94) was detected only in UM22Bap1$^{+/+}$ and UM22Bap1$^{-/-}$ cells, Flotilin-1 was found both in UM cells and SEVs. Finally, CD63 and CD9 were detected only in SEVs (Fig. 20 C), thus confirming the EV nature of our samples.

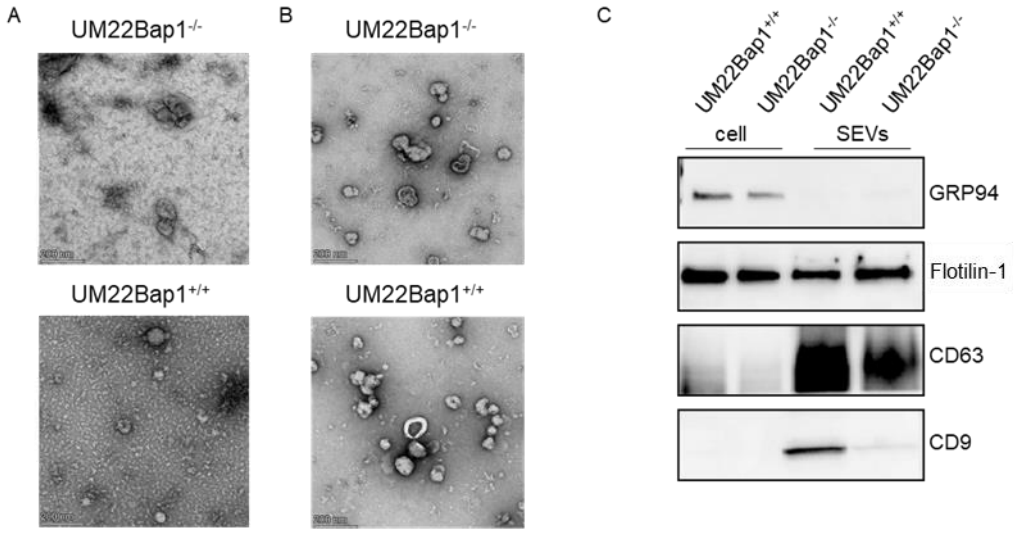

FIGURE 20 UM_SEVs characterization. SEVs were isolated from the conditioned media of UM22Bap1$^{+/+}$ and UM22Bap1$^{-/-}$ and characterization by TEM (A) before and (B) after the iodixanol density cushion ultracentrifugation. 5 µg of SEVs were loaded onto grids, negative stained, and evaluated by TEM. (C) Western blot was used to determine the presence of the CD9, CD63, Flottilin-1, and GRP94 in UM22Bap1$^{+/+}$ and UM22Bap1$^{-/-}$ cell and SEVs lysates.

4.6 UM_SEVs may induce EMT in healthy hepatocytes

In previous results, it was found that CRC_SEVs induced an EMT in normal heps, and vimentin, a mesenchymal marker, was strongly upregulated in CRC_SEVs treated heps compared to untreated cells. Interestingly, we observed an upregulation of vimentin also in heps treated with UM_SEVs for 24 and 48h (Fig. 21). In particular, after 48h of treatment only SEVs isolated from UM22Bap1$^{-/-}$ cells increased the protein expression of vimentin, thus suggesting that BAP1 mutation may play a role in liver metastasis by inducing an EMT in normal heps.

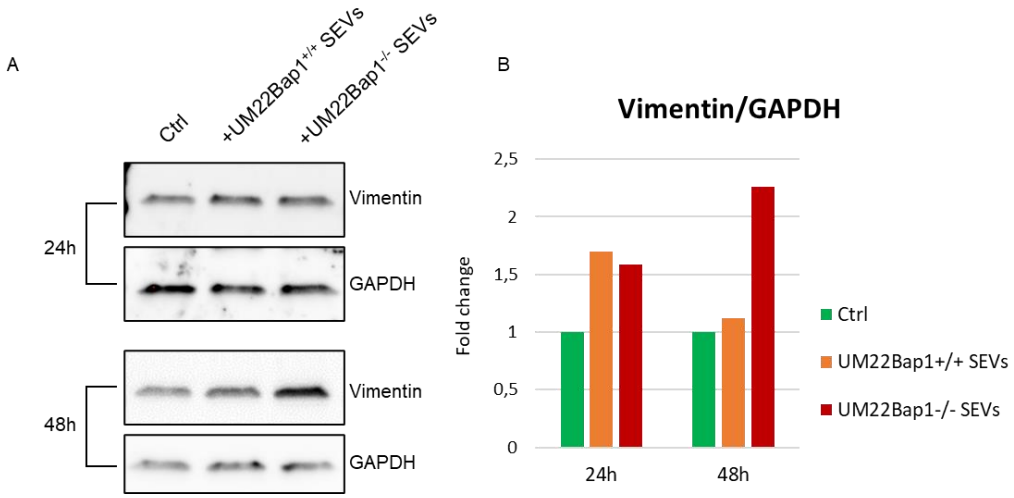

FIGURE 21 UM_SEVs effects on THLE-2 cells (A) Western blot analyses of vimentin in hepatocytes treated with UM22Bap1$^{+/+}$ and UM22Bap1$^{-/-}$ SEVs for 24 and 48h with (B) corresponding densitometric analyses.

4.7 3D model development

To further study the effects of CRC_SEVs in healthy heps and investigate the fibrotic process, which is known to drive metastatic cascade in the liver [132], a 3D cell culture model was developed. THLE-2 cells were seeded in ultra-low attachment 96 well plate and liver spheroids were obtained as described in the Material and Methods section (Fig. 22 A). The morphology of liver spheroids was analyzed through SEM, thanks to a collaboration with Prof. Guerrera of the University of Messina, thus demonstrating that the selected protocol allowed us to obtain good-shaped spheres with an average size of 100 μm (Fig. 22 B). The confocal analyses of the whole liver spheroids allowed us to better analyse liver spheroids morphology and confirm their size, about 120μm (Fig. 22 C). Liver spheroids were also sliced and stained with haematoxylin eosin as shown in Fig. 22 D, to confirm spheroids compactness and the absence of necrotic areas inside the 3D structure. In order to further characterize liver spheroids, we analysed the expression of HNF4 and E-cadherin (Fig. 22 E). The strong expression of HNF4 suggest that the 3D model obtained was well differentiated; while the expression of E-cadherin, a known cell-cell adhesion molecule [133], is in line with the high compactness of the 3D structure.

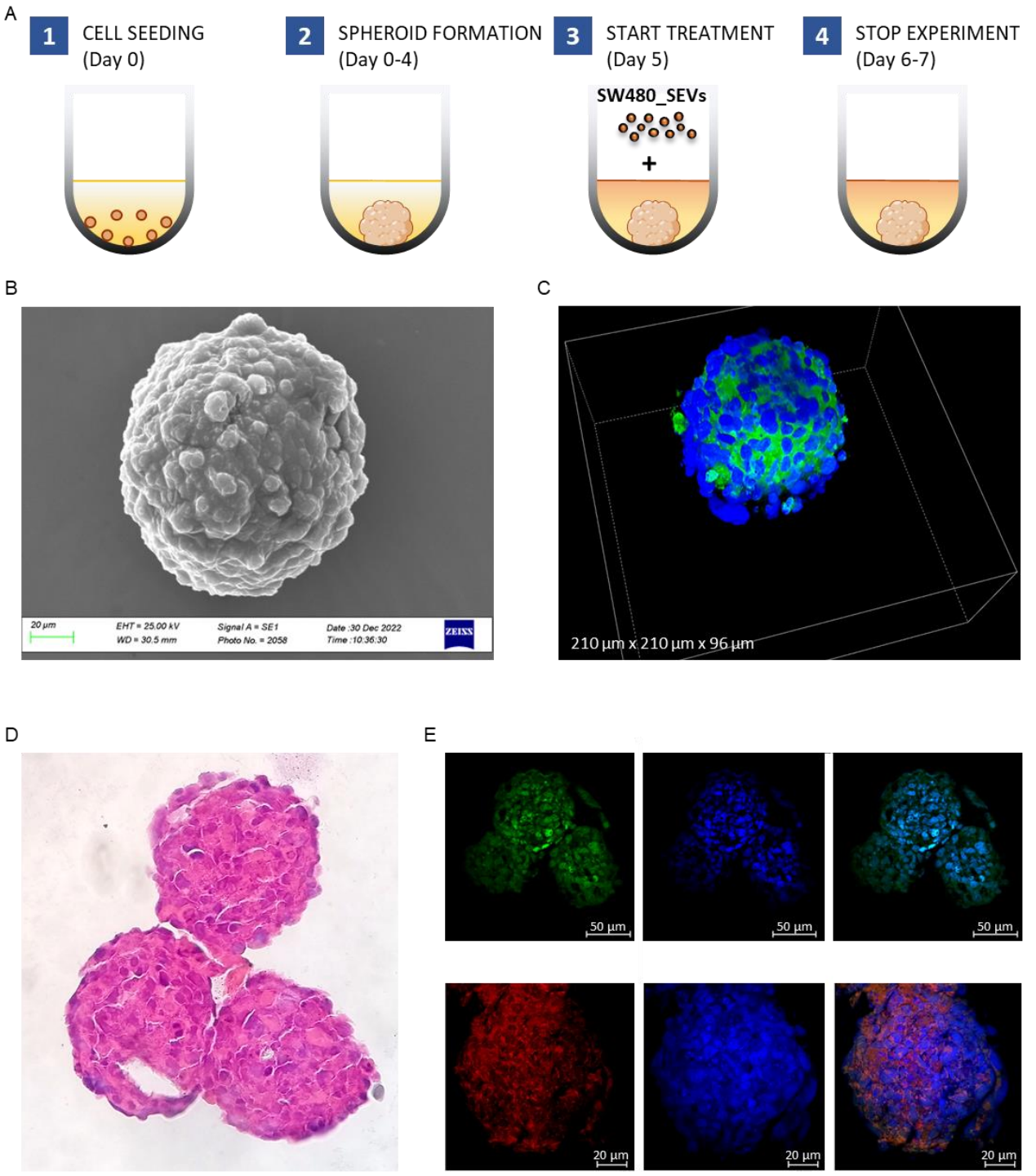

FIGURE 22 Characterization of liver spheroids. (A) Schematic illustration of the protocol used to grow liver spheroids using ultra-low attachment 96 well plate. (B) Scanning electron microscope micrograph of liver spheroid. Scale bars is 20 µm. (C) Confocal analysis of the whole liver spheroid: nuclei in blue and actin in green. The three dimensions are 210 µm x 210 µm x 96 µm. (D) Slices of liver spheroids stained with hematoxylin and eosin. (E, upper panel) Confocal analysis of liver spheroid slices, HNF4 in green and nuclei in blue. Scale bars are 50 µm. (E, lower panel) Confocal analysis of liver spheroid slices, E-Cadherin in red and nuclei in blue. Scale bars are 20 µm.

4.8 CRC_SEVs modulate the expression of hepatocytes markers in liver spheroids

Once we successfully set up the protocol to get good-shaped and functional liver spheroids, we tested the effect of CRC_SEVs on this model. Since the aim was to understand what happen to the hepatocytes when EVs from primary tumor arrive in the liver, for the following experiment the effect of only SW480-derived SEVs treatment were analysed. As first step, the internalization of SEVs derived from SW480 cells was investigated using confocal microscope. As shown in Fig. 23, after 3 and 6h of incubation SW480_SEVs were almost exclusively internalized by cells of the outer layers of the liver spheroids; while after 8h, SW480_SEVs were localized in the inner layers of the 3D structures. These data suggest that in 3D models EVs take more time to penetrate in all the cells than in 2D models, where sometime after 1h the uptake of EVs is already visible.

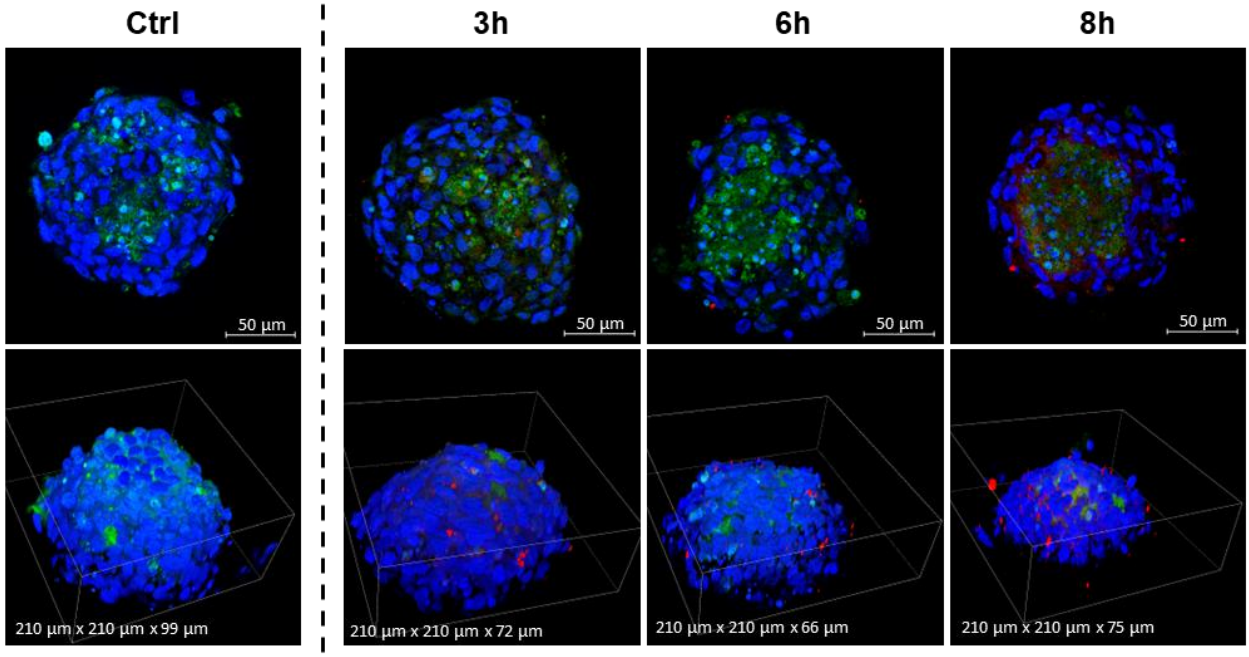

FIGURE 23 SW480_SEVs internalization by liver spheroids. SW480_SEVs were stained with PKH26 (in red) and incubated for 3, 6, and 8h. Actin was stained with Actin Green (in green) and nuclei with Hoechst (in blue). Scale bars are 50 µm.

Next, we examined the viability and cytotoxicity of liver spheroids following the treatment with SW480_SEVs to ensure that also in this model CRC_SEVs did not alter hepatocytes vitality. Not surprisingly, we demonstrated that SW480_SEVs treatment did not affect liver spheroids viability and did not induce toxicity (Fig. 24 A and B). To understand whether this 3D model was able to respond to CRC_SEVs and hepatocytes in 3D were affected by this treatment as well as they were in 2D the expression of hepatic functional markers was tested. As shown in Fig. 24 C, SW480_SEVs treatment downregulated the gene expression of ApoE and ALB.

The downregulation of ALB was confirmed at protein level through ELISA assay (Fig. 24 D). Moreover, SW480_SEVs reduced the protein expression of HNF4, which is known to drive and maintain hepatic differentiation, thus suggesting that CRC_SEVs impair hepatic functions (Fig. 24 E). Finally, the expression of CK8/18 was analysed through Western Blot and it was found that SW480_SEVs reduced CK8/18 expression compared to control condition (untreated liver spheroids). Overall, these data demonstrated that liver spheroids respond to CRC_SEVs treatment in a similar manner to heps grown in 2D. These results validate our previous data and highlight the validity of this model to study pre-metastatic niche formation in the liver.

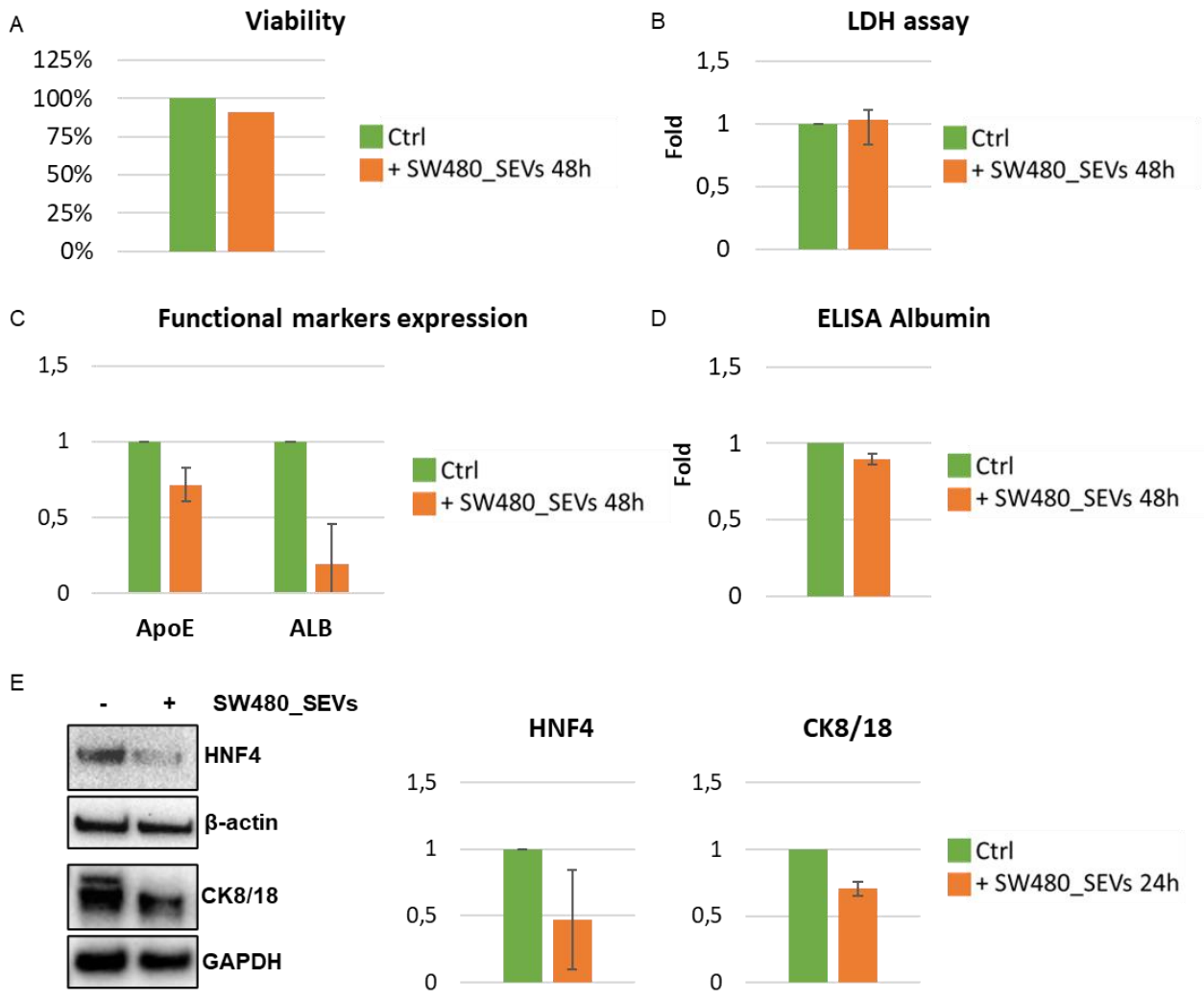

FIGURE 24 SW480_SEVs treatment affects the expression of functional and structural markers in liver spheroids. (A) Viability of liver spheroids treated with SW480_SEVs for 48h assessed with 3D Cell Titer Glo. (B) LDH release in the conditioned medium of liver spheroids treated with SW480_SEVs for 48h. (C) RT-qPCR of ApoE and ALB expression in liver spheroids treated with SW480_SEVs for 48h. (D) ELISA assay of ALB released in the conditioned medium of liver spheroids treated with SW480_SEVs for 48h. (E) Western blot analyses of HNF4 and CK8/18 in liver spheroids treated with SW480_SEVs for 24 h and corresponding densitometric analyses. The values are the mean (±SD) from two independent experiments.

4.9 CRC_SEV-educated liver spheroids favour CRC metastatic cells invasion

Our previous results demonstrated that CRC_SEVs induce an EMT on healthy heps and although fibrosis is linked to EMT it was not possible to study the deposition of extracellular matrix (ECM) proteins due to the limitations of the 2D model. In particular, as described in the Material and Methods section, THLE-2 cells grow in flasks coated with a solution made with fibronectin and collagen, making tricky the analysis of these molecules. The 3D model allowed us to overcome this limitation since cells growing in 3D do not need a coating and produce their own ECM [134]. In order to study the deposition of ECM proteins, liver spheroids were treated with SW480_SEVs for 48h, and the expression of fibronectin, known to be a marker of fibrosis in the metastatic liver [132], was analyzed through confocal microscope. As shown in Fig. 25, the expression of fibronectin was strongly increasing in liver spheroids treated with SW480_SEVs compared to the control condition, thus suggesting that CRC_SEVs may enhance the deposition of ECM proteins and favour liver fibrosis that in turn can lead to metastasis.

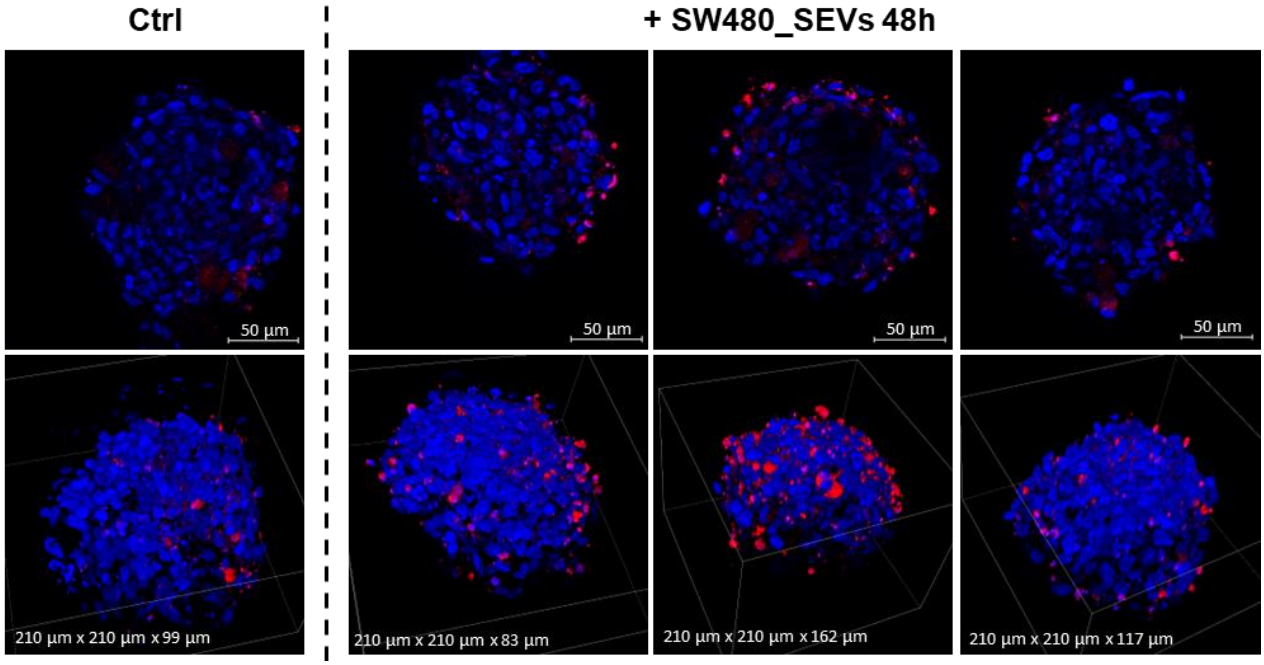

FIGURE 25 SW480_SEVs induce the deposition of ECM protein in liver spheroids. Confocal analysis of fibronectin (in red) in liver spheroids treated with SW480_SEVs for 48h. Nuclei were stained in blue with Hoechst. Scale bars are 50 µm.

To investigate the ability of CRC_SEVs to educate liver spheroids and modify their structure to accommodate metastatic CRC cells a 3D model of invasion was set up, based on the co-culture of liver spheroids and SW620 cells. For this experiment, the SW620 cell line was selected because it is isolated from lymph nodes and it is known to do metastasis *in vivo* [135].

The idea was to mimic what may happen *in vivo*: SEVs from the primary tumor (SW480 cells) reach the liver and educate it ("seed and soil" theory), then metastatic cells (SW620 cells) enter into the liver and invade it. Following 72h of treatment with SW480_SEVs, we added SW620 cells to liver spheroid. The invasion of SW620 cells in liver spheroids was evaluated after 24h of co-culturing (Fig. 26 A). Confocal analysis revealed that while in control liver spheroids SW620 cells made contact with only out-layer cells of the spheroids, SW480_SEVs pre-conditioning promoted the invasion of SW620 cells in the inner layers of liver spheroids (Fig. 26 B). These results highlight that CRC_SEVs affect the phenotype of heps favouring the establishment of a pre-metastatic niche seeding the soil for the metastatic cells.

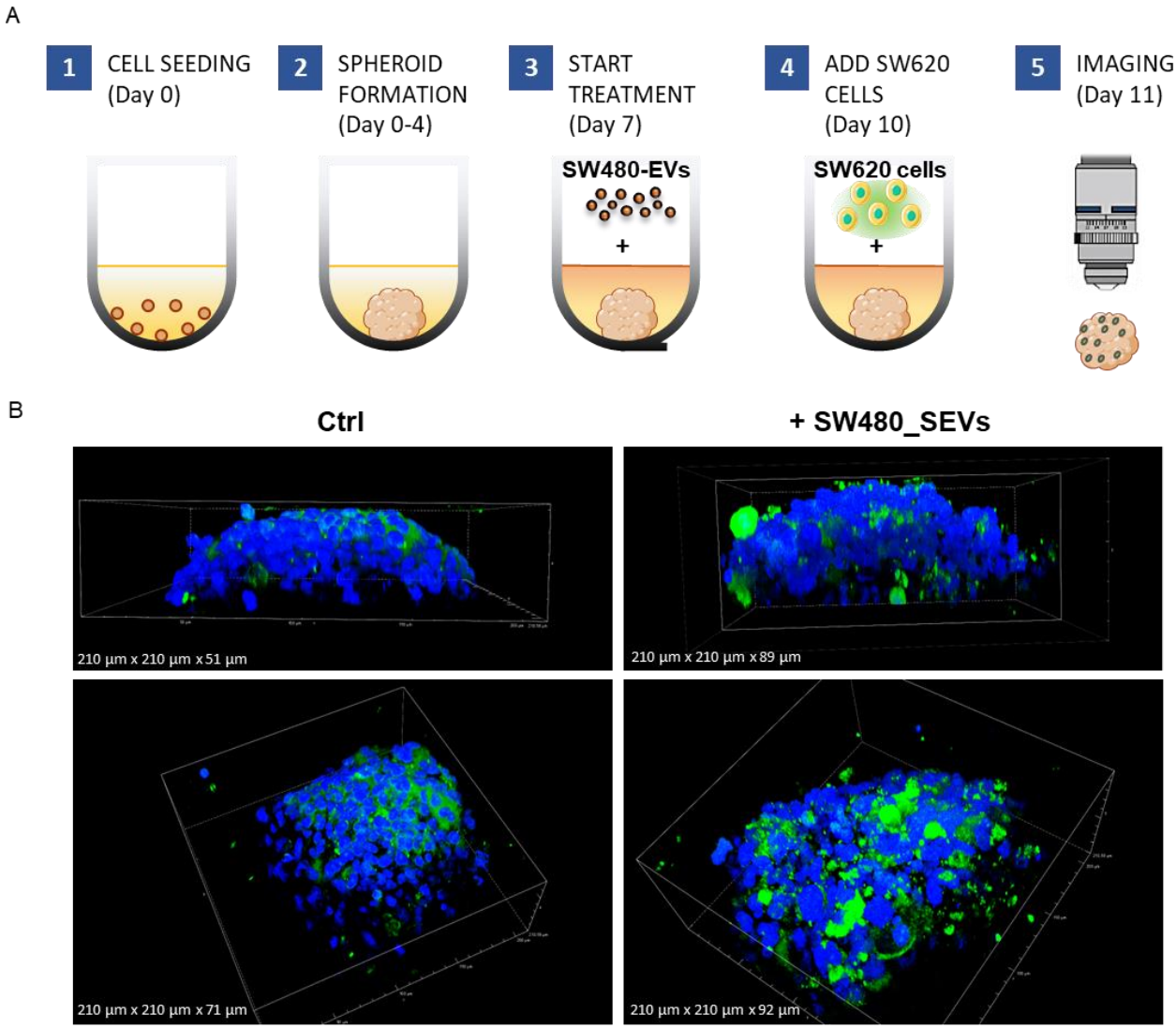

FIGURE 26 SW480_SEVs favour the invasion of metastatic cells in liver spheroids. (A) Schematic illustration of the protocol used to analyze the invasion of SW620-GFP cells into liver spheroids: following 72h of treatment with SW480_SEVs, SW620-GFP cells were co-cultured with liver spheroids for 24h. (B) Confocal analysis of SW620 cells (in green) invasion in liver spheroids pre-treated with SW480_SEVs for 72h. Nuclei were stained in blue with Hoechst. The three dimensions are indicated in the figures.

5. Discussion

Accumulating evidence suggests that EVs released by primary tumor cells are key players in regulation of the metastatic process, including the early step driving to the formation of the pre-metastatic niche [20, 98, 100, 136]. TD-SEVs can reach and alter secondary sites before tumor cell arrival, conditioning the pre-metastatic niche via immunosuppression, macrophage polarization, angiogenesis, stromal cell remodeling, and oncogenic reprogramming [100, 137-139]). In the liver it has been described that TD-SEVs lead to the formation of a fibrotic and immunosuppressive pre-metastatic niche directly targeting Kupffer cells, hepatic stellate cells and natural killer cells, while no data are available about the involvement of heps [98, 140, 141]. In this study we provided the first evidence that CRC-derived SEVs directly affect the phenotypic traits of heps. We found that CRC_SEVs carrying TGFβ1 elicit a decrease in hepatocyte marker genes (HNF4, albumin, APOE, and CYP3A4) and the activation of a TGFβ1/SMAD-dependent EMT associated with the acquisition of mesenchymal markers (vimentin and a-SMA) and with a reduction of epithelial marker expression (CK8/18 and E-cadherin). Our findings suggest a new role of TGFβ1-carrying CRC_SEVs in inducing an early alteration of structural and functional properties of liver parenchyma, thus anticipating the liver damage often associated with metastasis and leading heps to EMT described as an early step of fibrinogenesis [53].

Here we demonstrated that CRC_SEVs carry TGFβ1 in CRC_SEVs and using super resolution microscopy we found that TGFβ1 is located on the surface of CRC_SEVs. The surface localization of TGFβ1 was further confirmed by treating the SEVs with trypsin, thus making undetectable TGFβ1 in CRC_SEVs. The association of TGFβ1 with SEVs surface may be mediated by transforming growth factor beta receptor 3 (TGFBR3), which was previously identified in the proteome of CRC_SEVs by our group [90]. On the other hand, TGFβ1 could be just sticked on SEVs surface without a specific interaction. An elegant study by Lötvall´s group demonstrated that TGFβ1 is associated to EV surface through heparinase-II and pH-sensitive elements, which could be another mechanism of association of TGFβ1 with CRC_SEVs. Further studies are needed to clarify how TGFβ1 is associated to CRC_SEVs surface.

TGFβ1 is reported as a central player of liver injury able to induce decrease in several adult hepatocyte markers, such as HNF-4α and albumin, thus affecting the hepatic-specific functions [117, 118]. Moreover, TGFβ1 is described as one of stronger signals that can regulate cell plasticity, inducing EMT-associated modifications of the different liver cell populations, including hepatic stellate cells and hepatocytes, thus contributing to liver fibrosis [41, 53, 142]. Hepatic fibrosis is a non-physiological process characterized by excessive ECM, which causes tissue damage and failure or alteration of proper liver function.

It is considered a key driver of chronic liver injury, and the fibrosis niche is described as a favorable microenvironment for metastatic formation in the liver. Moreover, recent studies have reported that liver fibrosis is a powerful negative predictor of hepatic-specific disease-free survival and relapse-free survival in CRC [42]. Even if hepatic stellate cells are widely considered the main matrix-producing cells that drive liver fibrosis, evidence from several *in vitro* and *in vivo* studies suggests that TGFβ1-stimulated heps can undergo phenotypic and functional changes and can acquire a fibroblast-like morphology leading them to EMT associated with liver fibrosis [143, 144]. However, since some contradictory results have questioned the EMT of heps and its contribution to liver fibrogenesis [145], the debate is still open, and numerous studies are focused on this topic [144].

Recently, it has been reported that during the pro-metastatic process, heps actively participate to alter the immune and fibrotic microenvironment of the liver, inducing the activation of IL-6/STAT3 signaling and the subsequent production of serum amyloid A1 and A2 [146]. Our study, demonstrating that CRC_SEVs elicit heps to undergo EMT, points out an early potential activation of their pro-fibrotic behavior that can contribute to shape an environment supporting tumor cell colonization.

The preliminary results obtained in collaboration with the University of Gothenburg (Sweden) enforced the hypothesis that hepatocytes EMT could be also involved in liver metastasis of another type of cancer, uveal melanoma. Interestingly, using two different UM cell lines, with wild type or mutated BAP1 gene, it was possible to compare the effect of the respective secreted EVs on heps phenotype. The observed results suggest that BAP1 mutation may lead to the release of EVs that upregulated vimentin more than EVs released by wild type BAP1 cells. BAP1 mutations have been strongly associated with metastasis in UM patients [107, 147, 148]; we speculated that BAP1 mutation could affect EVs content thereby increasing metastatic potential.

The increased cell-cell and cell-ECM interactions made 3D cell cultures election models for the study of many biological processes, bridging the gap between *in vitro* and *in vivo* research [149]. We set up a protocol to obtain functional liver spheroids with a compact shape and morphology to investigate the fibrotic phenotype induced by CRC_SEVs. Although the interest in 3D models is growing in the last years, we are among the first groups which analysed the internalization of EVs in spheroids. Once validating the findings obtained with 2D model, the development of the 3D model allowed us to explore how the CRC_SEV-mediated EMT of heps can contribute to the formation of a fibrotic and tumor supportive microenvironment [150]. The strong increase in fibronectin deposition caused by CRC_SEVs treatment is clear evidence of the involvement of EVs in pre-metastatic niche priming. Interestingly, the liver metastasis-specific ECM signature included collagen VI, tenascin-C, collagen VI and collagen XIV, fibronectin and fibrinogens [132].

Taking inspiration from the work by the group of Gopalakrishnan [151], we set up our co-culture experiment to understand whether CRC_SEVs pre-treatment can affect the subsequence invasion of metastatic cells. The obtained results are the proof that the phenotypic changes induced by CRC_SEVs have a strong biological outcome when pre-conditioned liver cells encounter CRC metastatic cells.

Since metastasis is a complex mechanism in which many other factors are involved (e.g., organotropism, specific uptake in the organ, modulation of several cell phenotypes), further studies using *in vivo* models will be mandatory to assure the implication of CRC_SEVs in determining the involvement of heps during liver pre-metastatic niche formation and the related consequences.

6. Conclusions

In conclusion, our study revealed that CRC_SEVs directly target heps in which trigger a TGFβ1-mediated EMT, suggesting for the first time that CRC_SEV-educated heps may have an active role in the early stage of CRC liver metastasis formation (Fig. 27). This new evidence may offer new insights to develop more effective targeted therapeutic approaches against the formation of hepatic metastases.

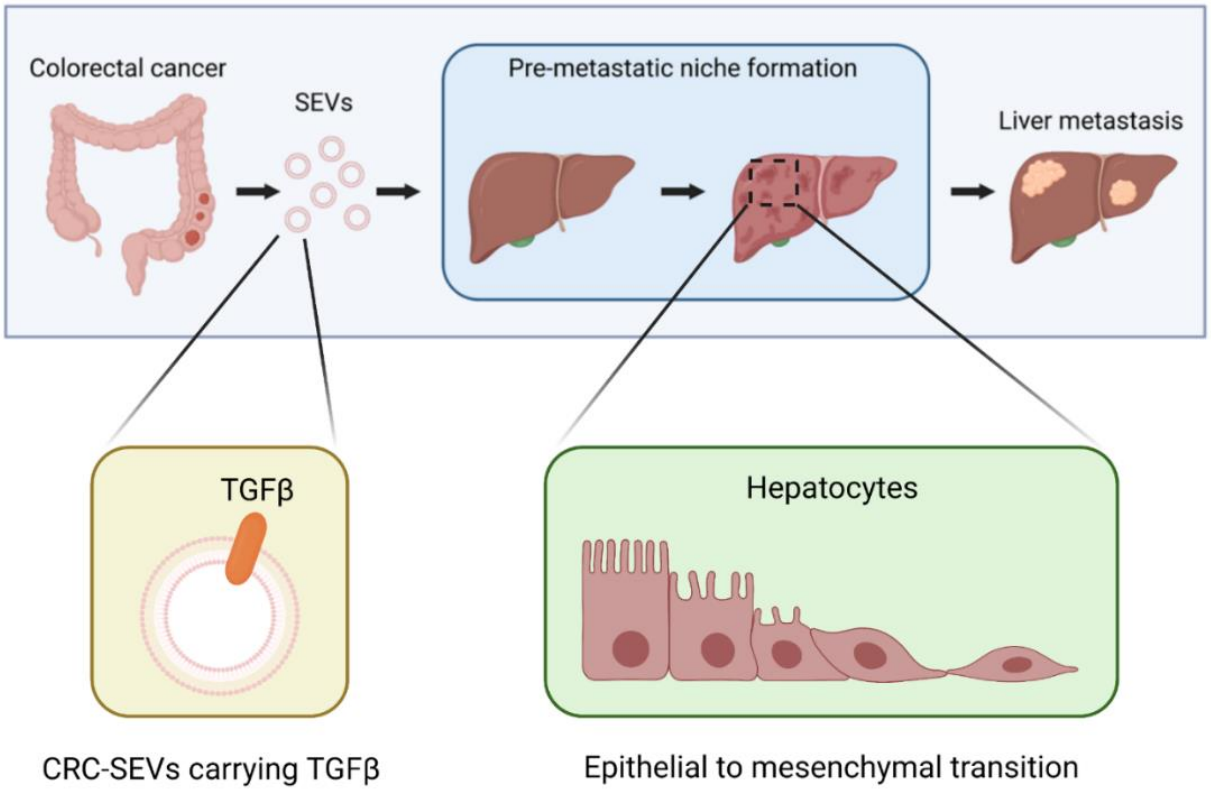

FIGURE 27 Schematic illustration of the results obtained in this study. Colorectal cancer cells release small extracellular vesicles (SEVs) carrying TGFβ. CRC_SEVs induce an EMT in healthy heps thereby taking part in the formation of the pre-metastatic niche in the liver. CRC: colorectal cancer; SEVs: small extracellular vesicles.

Bibliography

1. Raposo, G. et al. B lymphocytes secrete antigen-presenting vesicles. *J Exp Med* **183**, 1161-1172 (1996).
2. Sherr, C.J. Cancer cell cycles. *Science* **274**, 1672-1677 (1996).
3. Islami, F. et al. Proportion and number of cancer cases and deaths attributable to potentially modifiable risk factors in the United States. *CA Cancer J Clin* **68**, 31-54 (2018).
4. Anand, P. et al. Cancer is a preventable disease that requires major lifestyle changes. *Pharm Res* **25**, 2097-2116 (2008).
5. Hanahan, D. & Weinberg, R.A. Hallmarks of cancer: the next generation. *Cell* **144**, 646-674 (2011).
6. Hanahan, D. Hallmarks of Cancer: New Dimensions. *Cancer Discov* **12**, 31-46 (2022).
7. Zhao, D. et al. Histone Methyltransferase KMT2B Promotes Metastasis and Angiogenesis of Cervical Cancer by Upregulating EGF Expression. *Int J Biol Sci* **19**, 34-49 (2023).
8. Massague, J. & Obenauf, A.C. Metastatic colonization by circulating tumour cells. *Nature* **529**, 298-306 (2016).
9. van Zijl, F., Krupitza, G. & Mikulits, W. Initial steps of metastasis: cell invasion and endothelial transmigration. *Mutat Res* **728**, 23-34 (2011).
10. Fares, J., Fares, M.Y., Khachfe, H.H., Salhab, H.A. & Fares, Y. Molecular principles of metastasis: a hallmark of cancer revisited. *Signal Transduct Target Ther* **5**, 28 (2020).
11. Paget, S. The distribution of secondary growths in cancer of the breast. 1889. *Cancer Metastasis Rev* **8**, 98-101 (1989).
12. Yamamichi, G., Kato, T., Uemura, M. & Nonomura, N. Diagnosing and Prognosing Bone Metastasis in Prostate Cancer: Clinical Utility of Blood Biomarkers. *Anticancer Res* **43**, 283-290 (2023).
13. Bethlehem, M.S., Katsarelias, D. & Olofsson Bagge, R. Meta-Analysis of Isolated Hepatic Perfusion and Percutaneous Hepatic Perfusion as a Treatment for Uveal Melanoma Liver Metastases. *Cancers (Basel)* **13** (2021).
14. Khalil, D.T., Slater, K. & Cooper, C. Metastatic Breast Cancer Presenting as Acute Appendicitis. *Cureus* **14**, e30456 (2022).
15. Gao, Y. et al. Metastasis Organotropism: Redefining the Congenial Soil. *Dev Cell* **49**, 375-391 (2019).
16. Peinado, H. et al. Pre-metastatic niches: organ-specific homes for metastases. *Nat Rev Cancer* **17**, 302-317 (2017).
17. Psaila, B. & Lyden, D. The metastatic niche: adapting the foreign soil. *Nat Rev Cancer* **9**, 285-293 (2009).
18. Kaplan, R.N. et al. VEGFR1-positive haematopoietic bone marrow progenitors initiate the pre-metastatic niche. *Nature* **438**, 820-827 (2005).
19. Joyce, J.A. & Pollard, J.W. Microenvironmental regulation of metastasis. *Nat Rev Cancer* **9**, 239-252 (2009).
20. Dong, Q. et al. Pre-metastatic Niche Formation in Different Organs Induced by Tumor Extracellular Vesicles. *Front Cell Dev Biol* **9**, 733627 (2021).
21. Force, U.S.P.S.T. et al. Screening for Colorectal Cancer: US Preventive Services Task Force Recommendation Statement. *JAMA* **325**, 1965-1977 (2021).
22. Xi, Y. & Xu, P. Global colorectal cancer burden in 2020 and projections to 2040. *Transl Oncol* **14**, 101174 (2021).
23. Dai, X.C. et al. Calorie restriction remodels gut microbiota and suppresses tumorigenesis of colorectal cancer in mice. *Exp Ther Med* **25**, 59 (2023).
24. Holthuijsen, D.D.B. et al. Longitudinal Associations of Adherence to the Dietary World Cancer Research Fund/American Institute for Cancer Research (WCRF/AICR) and Dutch Healthy Diet (DHD) Recommendations with Plasma Kynurenines in Colorectal Cancer Survivors after Treatment. *Nutrients* **14** (2022).
25. Takahashi, K. et al. RNA editing is a valuable biomarker for predicting carcinogenesis in ulcerative colitis. *J Crohns Colitis* (2022).
26. Kuipers, E.J. et al. Colorectal cancer. *Nat Rev Dis Primers* **1**, 15065 (2015).
27. Jones, S. et al. Comparative lesion sequencing provides insights into tumor evolution. *Proc Natl Acad Sci U S A* **105**, 4283-4288 (2008).
28. Markowitz, S.D. & Bertagnolli, M.M. Molecular origins of cancer: Molecular basis of colorectal cancer. *N Engl J Med* **361**, 2449-2460 (2009).
29. Eefsen, R.L. et al. Therapy with pembrolizumab in treatment-naive patients with nonmetastatic, mismatch repair deficient colorectal cancer. *Int J Cancer* **152**, 2145-2152 (2023).
30. Raoux, L. et al. Impact of the strategy for curative treatment of synchronous colorectal cancer liver metastases. *J Visc Surg* **157**, 289-299 (2020).
31. Pan, Z. et al. Is there a survival benefit from adjuvant chemotherapy for patients with liver oligometastases from colorectal cancer after curative resection? *Cancer Commun (Lond)* **38**, 29 (2018).
32. Tsilimigras, D.I. et al. Liver metastases. *Nat Rev Dis Primers* **7**, 27 (2021).
33. Zhou, H. et al. Colorectal liver metastasis: molecular mechanism and interventional therapy. *Signal Transduct Target Ther* **7**, 70 (2022).
34. Hui, L. & Chen, Y. Tumor microenvironment: Sanctuary of the devil. *Cancer Lett* **368**, 7-13 (2015).

35. Liu, Y. & Cao, X. Characteristics and Significance of the Pre-metastatic Niche. *Cancer Cell* **30**, 668-681 (2016).
36. Wisse, E., De Zanger, R.B., Charels, K., Van Der Smissen, P. & McCuskey, R.S. The liver sieve: considerations concerning the structure and function of endothelial fenestrae, the sinusoidal wall and the space of Disse. *Hepatology* **5**, 683-692 (1985).
37. Matsumura, H. et al. Kupffer cells decrease metastasis of colon cancer cells to the liver in the early stage. *Int J Oncol* **45**, 2303-2310 (2014).
38. Keirsse, J. et al. The role of hepatic macrophages in liver metastasis. *Cell Immunol* **330**, 202-215 (2018).
39. Derynck, R. & Budi, E.H. Specificity, versatility, and control of TGF-beta family signaling. *Sci Signal* **12** (2019).
40. Ma, J., Sanchez-Duffhues, G., Goumans, M.J. & Ten Dijke, P. TGF-beta-Induced Endothelial to Mesenchymal Transition in Disease and Tissue Engineering. *Front Cell Dev Biol* **8**, 260 (2020).
41. Fabregat, I. & Caballero-Diaz, D. Transforming Growth Factor-beta-Induced Cell Plasticity in Liver Fibrosis and Hepatocarcinogenesis. *Front Oncol* **8**, 357 (2018).
42. Hu, X. et al. Prediction of hepatic metastasis and relapse in colorectal cancers based on concordance analyses with liver fibrosis scores. *Clin Transl Med* **9**, 13 (2020).
43. Cox, T.R. & Erler, J.T. Molecular pathways: connecting fibrosis and solid tumor metastasis. *Clin Cancer Res* **20**, 3637-3643 (2014).
44. Cox, T.R. et al. LOX-mediated collagen crosslinking is responsible for fibrosis-enhanced metastasis. *Cancer Res* **73**, 1721-1732 (2013).
45. Calon, A. et al. Stromal gene expression defines poor-prognosis subtypes in colorectal cancer. *Nat Genet* **47**, 320-329 (2015).
46. Hao, Y., Baker, D. & Ten Dijke, P. TGF-beta-Mediated Epithelial-Mesenchymal Transition and Cancer Metastasis. *Int J Mol Sci* **20** (2019).
47. Calon, A. et al. Dependency of colorectal cancer on a TGF-beta-driven program in stromal cells for metastasis initiation. *Cancer Cell* **22**, 571-584 (2012).
48. Tauriello, D.V.F. et al. TGFbeta drives immune evasion in genetically reconstituted colon cancer metastasis. *Nature* **554**, 538-543 (2018).
49. Yang, J. et al. Guidelines and definitions for research on epithelial-mesenchymal transition. *Nat Rev Mol Cell Biol* **21**, 341-352 (2020).
50. Thiery, J.P. & Sleeman, J.P. Complex networks orchestrate epithelial-mesenchymal transitions. *Nat Rev Mol Cell Biol* **7**, 131-142 (2006).
51. Lai, X. et al. Epithelial-Mesenchymal Transition and Metabolic Switching in Cancer: Lessons From Somatic Cell Reprogramming. *Front Cell Dev Biol* **8**, 760 (2020).
52. Dongre, A. & Weinberg, R.A. New insights into the mechanisms of epithelial-mesenchymal transition and implications for cancer. *Nat Rev Mol Cell Biol* **20**, 69-84 (2019).
53. Zhao, Y.L., Zhu, R.T. & Sun, Y.L. Epithelial-mesenchymal transition in liver fibrosis. *Biomed Rep* **4**, 269-274 (2016).
54. Martin-Taboada, M., Corrales, P., Medina-Gomez, G. & Vila-Bedmar, R. Tackling the effects of extracellular vesicles in fibrosis. *Eur J Cell Biol* **101**, 151221 (2022).
55. Pan, B.T. & Johnstone, R.M. Fate of the transferrin receptor during maturation of sheep reticulocytes in vitro: selective externalization of the receptor. *Cell* **33**, 967-978 (1983).
56. van Niel, G., D'Angelo, G. & Raposo, G. Shedding light on the cell biology of extracellular vesicles. *Nat Rev Mol Cell Biol* **19**, 213-228 (2018).
57. Fontana, S., Mauceri, R., Novara, M.E., Alessandro, R. & Campisi, G. Protein Cargo of Salivary Small Extracellular Vesicles as Potential Functional Signature of Oral Squamous Cell Carcinoma. *Int J Mol Sci* **22** (2021).
58. Cianciaruso, C. et al. Molecular Profiling and Functional Analysis of Macrophage-Derived Tumor Extracellular Vesicles. *Cell Rep* **27**, 3062-3080 e3011 (2019).
59. Raimondo, S. et al. Anti-inflammatory properties of lemon-derived extracellular vesicles are achieved through the inhibition of ERK/NF-kappaB signalling pathways. *J Cell Mol Med* **26**, 4195-4209 (2022).
60. Crescitelli, R. et al. Extracellular vesicle DNA from human melanoma tissues contains cancer-specific mutations. *Front Cell Dev Biol* **10**, 1028854 (2022).
61. Valadi, H. et al. Exosome-mediated transfer of mRNAs and microRNAs is a novel mechanism of genetic exchange between cells. *Nat Cell Biol* **9**, 654-659 (2007).
62. Raimondo, S. et al. Extracellular Vesicle microRNAs Contribute to the Osteogenic Inhibition of Mesenchymal Stem Cells in Multiple Myeloma. *Cancers (Basel)* **12** (2020).
63. Conigliaro, A. et al. CD90+ liver cancer cells modulate endothelial cell phenotype through the release of exosomes containing H19 lncRNA. *Mol Cancer* **14**, 155 (2015).
64. Gao, Y. et al. Small Extracellular Vesicles: A Novel Avenue for Cancer Management. *Front Oncol* **11**, 638357 (2021).
65. Xu, L. et al. Blood cell-derived extracellular vesicles: diagnostic biomarkers and smart delivery systems. *Bioengineered* **12**, 7929-7940 (2021).

66. Comfort, N. et al. Isolation and characterization of extracellular vesicles in saliva of children with asthma. *Extracell Vesicles Circ Nucl Acids* **2**, 29-48 (2021).
67. Merchant, M.L., Rood, I.M., Deegens, J.K.J. & Klein, J.B. Isolation and characterization of urinary extracellular vesicles: implications for biomarker discovery. *Nat Rev Nephrol* **13**, 731-749 (2017).
68. Muraoka, S. et al. Proteomic Profiling of Extracellular Vesicles Derived from Cerebrospinal Fluid of Alzheimer's Disease Patients: A Pilot Study. *Cells* **9** (2020).
69. Roca, J., Rodriguez-Martinez, H., Padilla, L., Lucas, X. & Barranco, I. Extracellular vesicles in seminal fluid and effects on male reproduction. An overview in farm animals and pets. *Anim Reprod Sci* **246**, 106853 (2022).
70. Admyre, C. et al. Exosomes with immune modulatory features are present in human breast milk. *J Immunol* **179**, 1969-1978 (2007).
71. Ciferri, M.C., Quarto, R. & Tasso, R. Extracellular Vesicles as Biomarkers and Therapeutic Tools: From Pre-Clinical to Clinical Applications. *Biology (Basel)* **10** (2021).
72. Tiwari, S., Kumar, V., Randhawa, S. & Verma, S.K. Preparation and characterization of extracellular vesicles. *Am J Reprod Immunol* **85**, e13367 (2021).
73. Crescitelli, R. et al. Distinct RNA profiles in subpopulations of extracellular vesicles: apoptotic bodies, microvesicles and exosomes. *J Extracell Vesicles* **2** (2013).
74. French, K.C., Antonyak, M.A. & Cerione, R.A. Extracellular vesicle docking at the cellular port: Extracellular vesicle binding and uptake. *Semin Cell Dev Biol* **67**, 48-55 (2017).
75. Cocucci, E. & Meldolesi, J. Ectosomes and exosomes: shedding the confusion between extracellular vesicles. *Trends Cell Biol* **25**, 364-372 (2015).
76. Cocucci, E., Racchetti, G. & Meldolesi, J. Shedding microvesicles: artefacts no more. *Trends Cell Biol* **19**, 43-51 (2009).
77. Xu, X., Lai, Y. & Hua, Z.C. Apoptosis and apoptotic body: disease message and therapeutic target potentials. *Biosci Rep* **39** (2019).
78. Lasser, C. et al. Two distinct extracellular RNA signatures released by a single cell type identified by microarray and next-generation sequencing. *RNA Biol* **14**, 58-72 (2017).
79. Kowal, J. et al. Proteomic comparison defines novel markers to characterize heterogeneous populations of extracellular vesicle subtypes. *Proc Natl Acad Sci U S A* **113**, E968-977 (2016).
80. Thery, C. et al. Minimal information for studies of extracellular vesicles 2018 (MISEV2018): a position statement of the International Society for Extracellular Vesicles and update of the MISEV2014 guidelines. *J Extracell Vesicles* **7**, 1535750 (2018).
81. Hill, A.F. Extracellular Vesicles and Neurodegenerative Diseases. *J Neurosci* **39**, 9269-9273 (2019).
82. de Abreu, R.C. et al. Native and bioengineered extracellular vesicles for cardiovascular therapeutics. *Nat Rev Cardiol* **17**, 685-697 (2020).
83. Akbar, N., Azzimato, V., Choudhury, R.P. & Aouadi, M. Extracellular vesicles in metabolic disease. *Diabetologia* **62**, 2179-2187 (2019).
84. Urabe, F. et al. Extracellular vesicles as biomarkers and therapeutic targets for cancer. *Am J Physiol Cell Physiol* **318**, C29-C39 (2020).
85. Bobrie, A. et al. Rab27a supports exosome-dependent and -independent mechanisms that modify the tumor microenvironment and can promote tumor progression. *Cancer Res* **72**, 4920-4930 (2012).
86. Matsumoto, A. et al. Accelerated growth of B16BL6 tumor in mice through efficient uptake of their own exosomes by B16BL6 cells. *Cancer Sci* **108**, 1803-1810 (2017).
87. Peinado, H. et al. Melanoma exosomes educate bone marrow progenitor cells toward a pro-metastatic phenotype through MET. *Nat Med* **18**, 883-891 (2012).
88. Antonyak, M.A. et al. Cancer cell-derived microvesicles induce transformation by transferring tissue transglutaminase and fibronectin to recipient cells. *Proc Natl Acad Sci U S A* **108**, 4852-4857 (2011).
89. Kreger, B.T., Dougherty, A.L., Greene, K.S., Cerione, R.A. & Antonyak, M.A. Microvesicle Cargo and Function Changes upon Induction of Cellular Transformation. *J Biol Chem* **291**, 19774-19785 (2016).
90. Schillaci, O. et al. Exosomes from metastatic cancer cells transfer amoeboid phenotype to non-metastatic cells and increase endothelial permeability: their emerging role in tumor heterogeneity. *Sci Rep* **7**, 4711 (2017).
91. Kreger, B.T., Johansen, E.R., Cerione, R.A. & Antonyak, M.A. The Enrichment of Survivin in Exosomes from Breast Cancer Cells Treated with Paclitaxel Promotes Cell Survival and Chemoresistance. *Cancers (Basel)* **8** (2016).
92. Yang, Y.H., Mao, J.W. & Tan, X.L. Research progress on the source, production, and anti-cancer mechanisms of paclitaxel. *Chin J Nat Med* **18**, 890-897 (2020).
93. Al-Nedawi, K., Meehan, B., Kerbel, R.S., Allison, A.C. & Rak, J. Endothelial expression of autocrine VEGF upon the uptake of tumor-derived microvesicles containing oncogenic EGFR. *Proc Natl Acad Sci U S A* **106**, 3794-3799 (2009).
94. Arum, C.J. et al. Cancer immunoediting from immunosurveillance to tumor escape in microvillus-formed niche: a study of syngeneic orthotopic rat bladder cancer model in comparison with human bladder cancer. *Neoplasia* **12**, 434-442 (2010).

95. Pucci, M. et al. Tumor-Derived Small Extracellular Vesicles Induce Pro-Inflammatory Cytokine Expression and PD-L1 Regulation in M0 Macrophages via IL-6/STAT3 and TLR4 Signaling Pathways. *Int J Mol Sci* **22** (2021).
96. Serrati, S. et al. Circulating extracellular vesicles expressing PD1 and PD-L1 predict response and mediate resistance to checkpoint inhibitors immunotherapy in metastatic melanoma. *Mol Cancer* **21**, 20 (2022).
97. Lucotti, S., Kenific, C.M., Zhang, H. & Lyden, D. Extracellular vesicles and particles impact the systemic landscape of cancer. *EMBO J* **41**, e109288 (2022).
98. Costa-Silva, B. et al. Pancreatic cancer exosomes initiate pre-metastatic niche formation in the liver. *Nat Cell Biol* **17**, 816-826 (2015).
99. Adem, B., Vieira, P.F. & Melo, S.A. Decoding the Biology of Exosomes in Metastasis. *Trends Cancer* **6**, 20-30 (2020).
100. Hoshino, A. et al. Tumour exosome integrins determine organotropic metastasis. *Nature* **527**, 329-335 (2015).
101. Tian, F. et al. Exosome-delivered miR-221/222 exacerbates tumor liver metastasis by targeting SPINT1 in colorectal cancer. *Cancer Sci* **112**, 3744-3755 (2021).
102. Shao, Y. et al. Colorectal cancer-derived small extracellular vesicles establish an inflammatory premetastatic niche in liver metastasis. *Carcinogenesis* **39**, 1368-1379 (2018).
103. Shang, A. et al. Exosomal miR-183-5p promotes angiogenesis in colorectal cancer by regulation of FOXO1. *Aging (Albany NY)* **12**, 8352-8371 (2020).
104. Zhang, C. et al. Cancer-derived exosomal HSPC111 promotes colorectal cancer liver metastasis by reprogramming lipid metabolism in cancer-associated fibroblasts. *Cell Death Dis* **13**, 57 (2022).
105. Wang, D. et al. Exosome-encapsulated miRNAs contribute to CXCL12/CXCR4-induced liver metastasis of colorectal cancer by enhancing M2 polarization of macrophages. *Cancer Lett* **474**, 36-52 (2020).
106. Zhao, S. et al. Tumor-derived exosomal miR-934 induces macrophage M2 polarization to promote liver metastasis of colorectal cancer. *J Hematol Oncol* **13**, 156 (2020).
107. Karlsson, J. et al. Molecular profiling of driver events in metastatic uveal melanoma. *Nat Commun* **11**, 1894 (2020).
108. Urzì, O. et al. Heat inactivation of foetal bovine serum causes protein contamination of extracellular vesicles. *bioRxiv*, 2023.2003.2001.530627 (2023).
109. Crescitelli, R., Lasser, C. & Lotvall, J. Isolation and characterization of extracellular vesicle subpopulations from tissues. *Nat Protoc* **16**, 1548-1580 (2021).
110. Crescitelli, R. et al. Subpopulations of extracellular vesicles from human metastatic melanoma tissue identified by quantitative proteomics after optimized isolation. *J Extracell Vesicles* **9**, 1722433 (2020).
111. Nizamudeen, Z. et al. Rapid and accurate analysis of stem cell-derived extracellular vesicles with super resolution microscopy and live imaging. *Biochim Biophys Acta Mol Cell Res* **1865**, 1891-1900 (2018).
112. Shelke, G.V. et al. Endosomal signalling via exosome surface TGFbeta-1. *J Extracell Vesicles* **8**, 1650458 (2019).
113. Cone, A.S. et al. Alix and Syntenin-1 direct amyloid precursor protein trafficking into extracellular vesicles. *BMC Mol Cell Biol* **21**, 58 (2020).
114. Olsavsky Goyak, K.M., Laurenzana, E.M. & Omiecinski, C.J. Hepatocyte differentiation. *Methods Mol Biol* **640**, 115-138 (2010).
115. Varghese, D.S., Alawathugoda, T.T. & Ansari, S.A. Fine Tuning of Hepatocyte Differentiation from Human Embryonic Stem Cells: Growth Factor vs. Small Molecule-Based Approaches. *Stem Cells Int* **2019**, 5968236 (2019).
116. Watt, A.J., Garrison, W.D. & Duncan, S.A. HNF4: a central regulator of hepatocyte differentiation and function. *Hepatology* **37**, 1249-1253 (2003).
117. Zeisberg, M. et al. Fibroblasts derive from hepatocytes in liver fibrosis via epithelial to mesenchymal transition. *J Biol Chem* **282**, 23337-23347 (2007).
118. Cicchini, C. et al. TGFbeta-induced EMT requires focal adhesion kinase (FAK) signaling. *Exp Cell Res* **314**, 143-152 (2008).
119. Yin, Y., Shelke, G.V., Lasser, C., Brismar, H. & Lotvall, J. Extracellular vesicles from mast cells induce mesenchymal transition in airway epithelial cells. *Respir Res* **21**, 101 (2020).
120. Ji, Y. et al. Multiplexed profiling of single-cell extracellular vesicles secretion. *Proc Natl Acad Sci U S A* **116**, 5979-5984 (2019).
121. Xu, J., Lamouille, S. & Derynck, R. TGF-beta-induced epithelial to mesenchymal transition. *Cell Res* **19**, 156-172 (2009).
122. Yastrebova, M.A., Khamidullina, A.I., Tatarskiy, V.V. & Scherbakov, A.M. Snail-Family Proteins: Role in Carcinogenesis and Prospects for Antitumor Therapy. *Acta Naturae* **13**, 76-90 (2021).
123. Xue, V.W. et al. Transforming Growth Factor-beta: A Multifunctional Regulator of Cancer Immunity. *Cancers (Basel)* **12** (2020).
124. Pucci, M. et al. Colorectal cancer-derived small extracellular vesicles induce TGFβ1-mediated epithelial to mesenchymal transition of hepatocytes. *Cancer Cell International* **23**, 77 (2023).

125. Bustamante, P., Piquet, L., Landreville, S. & Burnier, J.V. Uveal melanoma pathobiology: Metastasis to the liver. *Semin Cancer Biol* **71**, 65-85 (2021).
126. Hurst, E.A., Harbour, J.W. & Cornelius, L.A. Ocular melanoma: a review and the relationship to cutaneous melanoma. *Arch Dermatol* **139**, 1067-1073 (2003).
127. Gragoudas, E.S. et al. Survival of patients with metastases from uveal melanoma. *Ophthalmology* **98**, 383-389; discussion 390 (1991).
128. Sarosy, G., Leyland-Jones, B., Soochan, P. & Cheson, B.D. The systemic administration of intravenous melphalan. *J Clin Oncol* **6**, 1768-1782 (1988).
129. Ben-Shabat, I. et al. Isolated hepatic perfusion as a treatment for liver metastases of uveal melanoma. *J Vis Exp*, 52490 (2015).
130. Ravikumar, T.S. et al. Percutaneous hepatic vein isolation and high-dose hepatic arterial infusion chemotherapy for unresectable liver tumors. *J Clin Oncol* **12**, 2723-2736 (1994).
131. Louie, B.H. & Kurzrock, R. BAP1: Not just a BRCA1-associated protein. *Cancer Treat Rev* **90**, 102091 (2020).
132. Drew, J. & Machesky, L.M. The liver metastatic niche: modelling the extracellular matrix in metastasis. *Dis Model Mech* **14** (2021).
133. van Roy, F. & Berx, G. The cell-cell adhesion molecule E-cadherin. *Cell Mol Life Sci* **65**, 3756-3788 (2008).
134. LaBarbera, D.V., Reid, B.G. & Yoo, B.H. The multicellular tumor spheroid model for high-throughput cancer drug discovery. *Expert Opin Drug Discov* **7**, 819-830 (2012).
135. Hewitt, R.E. et al. Validation of a model of colon cancer progression. *J Pathol* **192**, 446-454 (2000).
136. Ghoroghi, S., Mary, B., Asokan, N., Goetz, J.G. & Hyenne, V. Tumor extracellular vesicles drive metastasis (it's a long way from home). *FASEB Bioadv* **3**, 930-943 (2021).
137. Feng, W., Dean, D.C., Hornicek, F.J., Shi, H. & Duan, Z. Exosomes promote pre-metastatic niche formation in ovarian cancer. *Mol Cancer* **18**, 124 (2019).
138. Rana, S., Yue, S., Stadel, D. & Zoller, M. Toward tailored exosomes: the exosomal tetraspanin web contributes to target cell selection. *Int J Biochem Cell Biol* **44**, 1574-1584 (2012).
139. Yuan, X. et al. Breast cancer exosomes contribute to pre-metastatic niche formation and promote bone metastasis of tumor cells. *Theranostics* **11**, 1429-1445 (2021).
140. Zhao, S. et al. Highly-metastatic colorectal cancer cell released miR-181a-5p-rich extracellular vesicles promote liver metastasis by activating hepatic stellate cells and remodelling the tumour microenvironment. *J Extracell Vesicles* **11**, e12186 (2022).
141. Zhang, H. et al. Exosome-delivered EGFR regulates liver microenvironment to promote gastric cancer liver metastasis. *Nat Commun* **8**, 15016 (2017).
142. Chen, Y. et al. Study on the relationship between hepatic fibrosis and epithelial-mesenchymal transition in intrahepatic cells. *Biomed Pharmacother* **129**, 110413 (2020).
143. Yu, K., Li, Q., Shi, G. & Li, N. Involvement of epithelial-mesenchymal transition in liver fibrosis. *Saudi J Gastroenterol* **24**, 5-11 (2018).
144. Zhu, J. et al. H19/miR-148a/USP4 axis facilitates liver fibrosis by enhancing TGF-beta signaling in both hepatic stellate cells and hepatocytes. *J Cell Physiol* **234**, 9698-9710 (2019).
145. Taura, K. et al. Hepatocytes do not undergo epithelial-mesenchymal transition in liver fibrosis in mice. *Hepatology* **51**, 1027-1036 (2010).
146. Lee, J.W. et al. Hepatocytes direct the formation of a pro-metastatic niche in the liver. *Nature* **567**, 249-252 (2019).
147. Harbour, J.W. et al. Frequent mutation of BAP1 in metastasizing uveal melanomas. *Science* **330**, 1410-1413 (2010).
148. Koopmans, A.E. et al. Clinical significance of immunohistochemistry for detection of BAP1 mutations in uveal melanoma. *Mod Pathol* **27**, 1321-1330 (2014).
149. Jensen, C. & Teng, Y. Is It Time to Start Transitioning From 2D to 3D Cell Culture? *Front Mol Biosci* **7**, 33 (2020).
150. Boulter, L., Bullock, E., Mabruk, Z. & Brunton, V.G. The fibrotic and immune microenvironments as targetable drivers of metastasis. *Br J Cancer* **124**, 27-36 (2021).
151. Goranci-Buzhala, G. et al. Rapid and Efficient Invasion Assay of Glioblastoma in Human Brain Organoids. *Cell Rep* **31**, 107738 (2020).

Acknowledgements

First and foremost, I would like to express my sincere gratitude to my supervisor, Prof. Simona Fontana, for her invaluable encouragement and continuous support during my PhD study. I am deeply grateful to Prof. Riccardo Alessandro, my mentor. His immense knowledge and precious advice have motivated me in all the time of my academic research and daily life. I would like to extend my sincere thanks to Prof. Alice Conigliaro, my sparkling source of inspiration, and Prof. Chiara Corrado, for her kind help and support. I will never thank Dr. Stefania Raimondo enough; she taught me everything: from how to pipette to how to carry out a research project. Most of the results shown here will never exist without Dr. Marzia Pucci, a clear example of a hard worker and beautiful soul. I would thank also Dr. Maria Antonietta Di Bella for her patience and determination. I would like to offer my special thanks to my colleagues Dr. Marilena Barreca, Dr. Liana Bosco, Aurora Cordaro, Elisa Costanzo, Nima Rabienezhad Ganji, Roberta Gasparro, Marco Loria, Dr. Marta Moschetti, Eugenia Novara, Vincenza Tinnirello, and Chiara Zichittella. Maybe because close contacts breed affection, I have to say that I love each of you. We spent hours and hours in lab, but there wasn´t a day when we didn´t laugh, joke or know that we could count on each other. Among my colleagues, Dr. Dragana Nikolic stole my heart; she is the proof that you should never give up, she is my dream colleague. I would like to extend my sincere thanks to the "guys" of IOR group, Dr. Daniele Bellavia, Dr. Valeria Carina, Dr. Viviana Costa, Dr. Angela De Luca, and Dr. Lavinia Raimondi, for their support and belief in me. I would like to thank all the students who I supervised, Anita Stassi, Selene Tranchida, Luigi Fiore, and Martina Vinci, they always thank me (maybe too much), but I have to thank them for treasuring what I tried to teach them.

I can happily say that all of them are my second family, and Via Divisi 83 is my second home.

The six months in Sweden were, probably, the icing on the cake of my PhD thanks to Dr. Rossella Crescitelli and Prof. Roger Olofsson Bagge. They made me grow and overcome my limitations, I will always carry them in my heart, tack!

I would like to express my gratitude to all my family, especially my parents, my brother and Molly who patiently listened to me when I had to repeat the presentations in the living room and let me talk about my exciting experiments during dinner. I would like to offer my special thanks to my grandparents, Mimma and Eugenio, my lovely first supporters.

Last but not least, I would thank my boyfriend, who not surprisingly I always put after so many things, so many experiments, so many thoughts, but he has always been by my side. Tolerating "Orni as PhD student" was perhaps the greatest challenge of his life and I can only love him for that reason.

PhD is a journey which cannot be faced alone, without each of you I would never have achieved this goal.